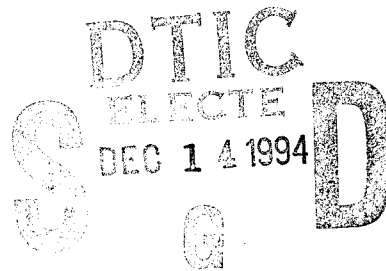


# NAVAL POSTGRADUATE SCHOOL MONTEREY, CALIFORNIA



## THESIS

### TECHNIQUES FOR THE INVESTIGATION OF WAVE TURBULENCE IN WATER WAVE DATA

By  
John P. Davies  
September 1994

Thesis Advisor:

Robert M. Keolian

Approved for public release; distribution is unlimited.

19941209 047

DTIC QUALITY INSPECTED 1

REPORT DOCUMENTATION PAGE			Form Approved OMB No. 0704-0188	
Public reporting burden for this collection of information is estimated to average 1 hour per response, including the time for reviewing instruction, searching existing data sources, gathering and maintaining the data needed, and completing and reviewing the collection of information. Send comments regarding this burden estimate or any other aspect of this collection of information, including suggestions for reducing this burden, to Washington Headquarters Services, Directorate for Information Operations and Reports, 1215 Jefferson Davis Highway, Suite 1204, Arlington, VA 22202-4302, and to the Office of Management and Budget, Paperwork Reduction Project (0704-0188) Washington DC 20503.				
1. AGENCY USE ONLY (Leave blank)	2. REPORT DATE September 1994	3. REPORT TYPE AND DATES COVERED Master's Thesis		
4. TITLE AND SUBTITLE TECHNIQUES FOR THE INVESTIGATION OF WAVE TURBULENCE IN WATER WAVE DATA		5. FUNDING NUMBERS		
6. AUTHOR(S) John P. Davies				
7. PERFORMING ORGANIZATION NAME(S) AND ADDRESS(ES) Naval Postgraduate School Monterey CA 93943-5000		8. PERFORMING ORGANIZATION REPORT NUMBER		
9. SPONSORING/MONITORING AGENCY NAME(S) AND ADDRESS(ES)		10. SPONSORING/MONITORING AGENCY REPORT NUMBER		
11. SUPPLEMENTARY NOTES. The views expressed in this thesis are those of the author and do not reflect the official policy or position of the Department of Defense or the U.S. Government.				
12a. DISTRIBUTION/AVAILABILITY STATEMENT Approved for public release; distribution is unlimited.		12b. DISTRIBUTION CODE A		
13. ABSTRACT (maximum 200 words) Computer based tools were developed to search water wave data for a collective mode predicted by wave turbulence theory. A low frequency wave, the "swell", can drive the collective mode by compressing and expanding the field of high frequency waves, the "chop". Through non-linear interactions, the chop responds with its own collective stiffness and inertia. This inertia should cause modulations of the chop amplitude to lag in phase behind the forcing from the swell. Two methods are presented for investigating the phase relationships between the chop amplitude and the swell. Method one employs the Fast Fourier Transform to examine directly the power levels at various frequencies. Method two employs digital signal processing to separate the swell and chop frequencies and the Hilbert Transform to compute the instantaneous phase of the swell and instantaneous amplitude of the chop. Various plotting techniques permit the examination of the relationships between the amplitude of the chop and the phase of the swell. The second method provided evidence of the collective mode when applied to data collected in a wave tank experiment described herein.				
14. SUBJECT TERMS Wave Turbulence, Collective Mode, Hilbert Transform		15. NUMBER OF PAGES 78		
		16. PRICE CODE		
17. SECURITY CLASSIFICATION OF REPORT Unclassified	18. SECURITY CLASSIFICATION OF THIS PAGE Unclassified	19. SECURITY CLASSIFICATION OF ABSTRACT Unclassified	20. LIMITATION OF ABSTRACT UL	



Approved for public release; distribution is unlimited.

**TECHNIQUES FOR THE INVESTIGATION OF  
WAVE TURBULENCE IN WATER WAVE DATA**

by

**John P. Davies**  
Lieutenant Commander, Canadian Forces  
B.Math, University of Waterloo, 1990

Submitted in partial fulfillment of the requirements for the  
degree of

**MASTER OF SCIENCE IN ENGINEERING ACOUSTICS**

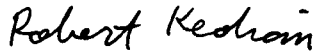
from the

**NAVAL POSTGRADUATE SCHOOL**  
**September, 1994**

Author:

  
John P. Davies

Approved by:



Robert M. Keolian, Thesis Advisor



Andres Larraza, Thesis Second Reader



James V. Sanders, Acting Chairman  
Engineering Acoustics Academic Committee

Accession For	
NTIS	CRA&I <input checked="" type="checkbox"/>
DTIC	TAB <input type="checkbox"/>
Unannounced Justification <input type="checkbox"/>	
By _____	
Distribution / _____	
Availability Codes	
Dist	Avail and/or Special
A-1	



## **ABSTRACT**

Computer based tools were developed to search water wave data for a collective mode predicted by wave turbulence theory. A low frequency wave, the "swell," can drive the collective mode by compressing and expanding the field of high frequency waves, the "chop." Through non-linear interactions, the chop responds with its own collective stiffness and inertia. This inertia should cause modulations of the chop amplitude to lag in phase behind the forcing from the swell.

Two methods are presented for investigating the phase relationships between the chop amplitude and the swell. Method one employs the Fast Fourier Transform to examine directly the power levels at various frequencies. Method two employs digital signal processing to separate the swell and chop frequencies and the Hilbert Transform to compute the instantaneous phase of the swell and instantaneous amplitude of the chop. Various plotting techniques permit the examination of the relationships between the amplitude of the chop and the phase of the swell. The second method provided evidence of the existence of the collective mode when applied to data collected in a wave tank experiment described herein.



## TABLE OF CONTENTS

I. INTRODUCTION .....	1
II. THE DATA.....	7
III. THE FAST FOURIER TRANSFORM APPROACH.....	11
A. INTRODUCTION .....	11
B. PROCEDURE.....	11
C. OBSERVATIONS .....	12
IV. THE HILBERT TRANSFORM APPROACH.....	21
A. INTRODUCTION .....	21
B. BACKGROUND.....	21
1. The Hilbert Transform.....	21
2. The Chebyshev Type II Filter .....	22
C. PROCEDURE.....	24
1. Filtering.....	24
2. Instantaneous Phase - Low Wave.....	26
3. Instantaneous Amplitude - High Wave .....	26
4. Plotting .....	26
5. Test Signal.....	27
D. OBSERVATIONS .....	30
1. Filtering - Wave Field Data .....	30
2. Scatter Diagram - Wave Field Data .....	34
3. Distribution Plot - Wave Field Data .....	39
4. Frequency Octave Band Analysis - Wave Field Data.....	41
5. Filtering - Wave Tank Data .....	47
6. Distribution Plot - Wave Tank Data .....	47



V. CONCLUSIONS AND FUTURE WORK.....	53
APPENDIX A. MATLAB CODE .....	55
APPENDIX B. WAVE TANK SIGN TEST .....	61
REFERENCES .....	65
INITIAL DISTRIBUTION LIST .....	67

## ACKNOWLEDGMENT

I would like to acknowledge the financial support of the Office of Naval Research, for funding the purchase of the computers and software used in this thesis.

I would also like to thank Patricia, my wife, and Elizabeth, my daughter, for giving me the time and space I needed to complete my studies and this thesis. I promise to spend more time with both of you when "daddy" doesn't have anymore homework.

I want to thank Lt. Patty Gill for running the tank experiments, it is a dirty job (literally) but someone has to do it, better you than me.

I want to thank Dr. Bob Keolian and Dr. Andy Larraza for their guidance over the past year. A special thanks to Dr. Bob for continually reminding me that we were pushing back the dark curtain of ignorance and shedding light on never before explored regions of science.

Finally, I'd like to thank my fellow travellers on this road of academic adventure, my to section mates Lt. Jan Fietz, USN and Lt. Warren Huelsnitz, USN, my office mate LCdr Dave Brenner, Cdn Forces and all the other voyagers. Thank you all for the help and support, together we made it through.



## I. INTRODUCTION

This thesis is part of a continuing experimental study (Lawrence, 1992) of wave turbulence (Zakharov, 1992), a theory of the non-linear interactions of a random sea of waves. In wave turbulence, as applied to the ocean surface, wind energy drives surface waves at a length scale determined by the wind speed. The energy is then redistributed through non-linear interactions to other surface waves of various lengths leading to an equilibrium wave energy spectrum. Energy proceeds through shorter wavelengths in a "forward cascade," leading to a predicted  $\omega^{-4}$  power law at the higher frequencies. This energy is ultimately absorbed by dissipation. At low frequencies, the energy from the wind progresses towards longer wavelengths through an "inverse cascade," leading to a predicted  $\omega^{-(11/4)}$  power law. The spectrum cuts off at the lowest frequencies because of limited fetch or basin size.

Larraza et al, (Larraza, 1990) and Larraza and Falkovich (Larraza, 1993) have studied what happens when this background energy distribution is disturbed or modulated spatially. Instead of the spectrum relaxing back to equilibrium exponentially, they have predicted that perturbations of the spectrum propagate in space as a collective mode. The mode is a *wave* in the *density of waves*, analogous somewhat to sound, a wave in the density of particles. Like sound, the mode propagates at a speed which is frequency independent, and the speed is nearly equal to the group velocity of the fastest components of the background spectrum, which for the collective mode are those low frequency waves near the spectral peak and for sound are those particles moving near the thermal velocity.

The dispersion relations, plots of the angular frequency  $\omega$  of a wave versus its wave number  $k$ , are given in Figure 1-1 for the collective mode and for ordinary gravity waves. For the collective mode,  $\omega = c_{cm} k$ , where  $c_{cm}$  is the speed of the collective mode, and for gravity waves,  $\omega^2 = gk$ , where  $g$  is the acceleration due to gravity. The two curves are seen to cross at point  $B$  in Figure 1-1.

The collective mode can be driven by a very low frequency wave, which we shall call the "swell." The horizontal component of the fluid element particle velocity associated with the swell convects along any short waves, which we shall call the "chop," riding on top of the swell. Let us first allow individual waves of the chop to interact with the swell, but not with each other. Where the swell's flow is converging or diverging, the chop would be compressing or expanding, respectively. For example, in a traveling swell wave, the rate of compression of the chop would be greatest on the swell's leading edge, zero at the swell's crest or trough, and negative on its trailing edge. The accumulated amplitude of the chop would be proportional to the time integral of the rate of compression, giving a  $\pi/2$  phase shift, which puts the maximum amplitude of the chop at the crest of the swell. The same result holds for a standing swell wave. In both cases, one should expect that like cork dust floating on the swell, the density of non interacting chop would be highest where the most fluid elements have accumulated due the swell, i.e. at the crest of the swell. Both the swell and the modulations of the chop will have the same wavelength and wave number. Figure 1-2(A) illustrates how this case might appear when plotted in the time domain.

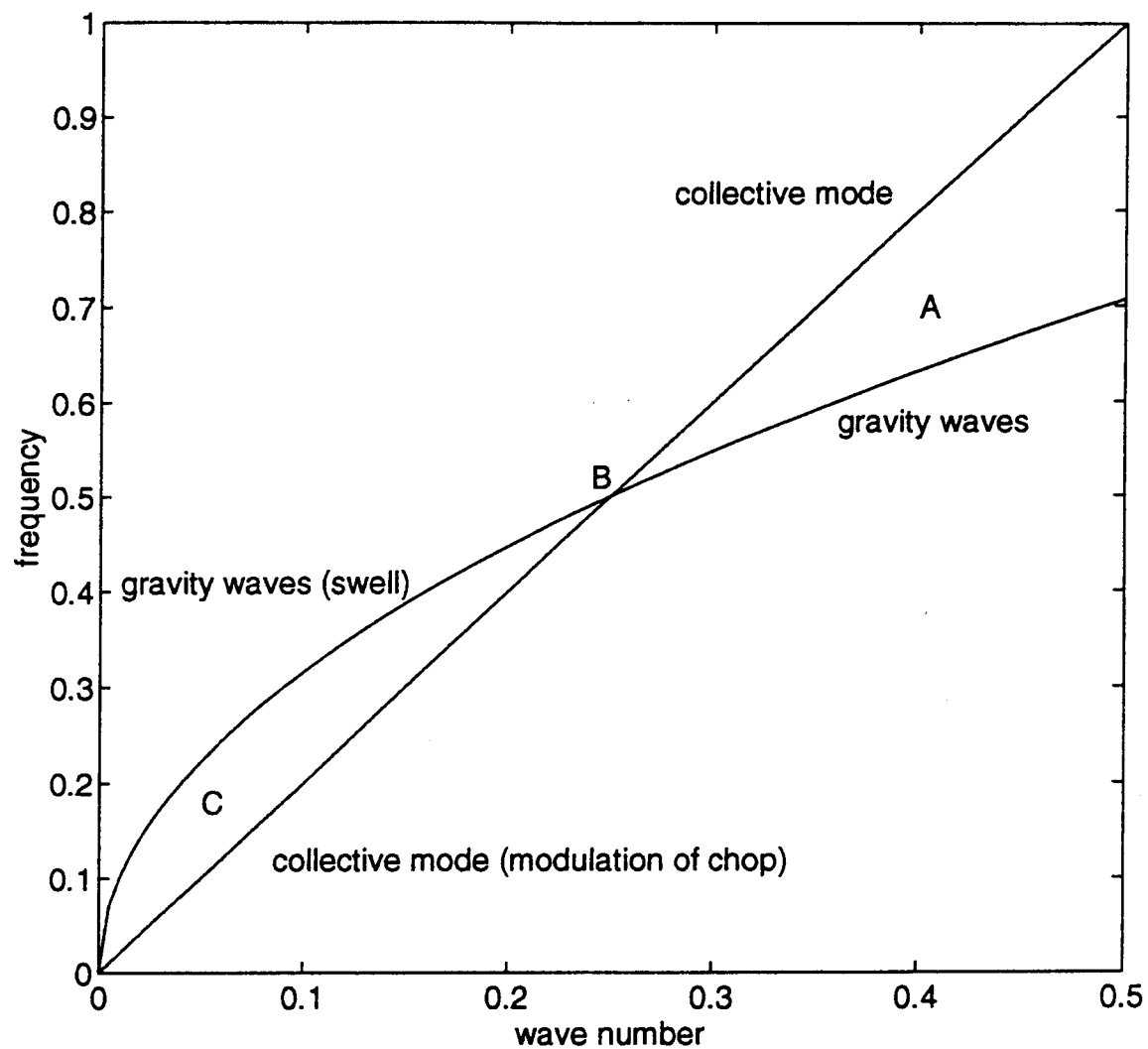


Figure 1-1. Dispersion Law  
Comparison of gravity waves and collective mode. Regions A, B, and C correspond to plots for lags of 0, 90 and 180 degrees in Figure 1-2.

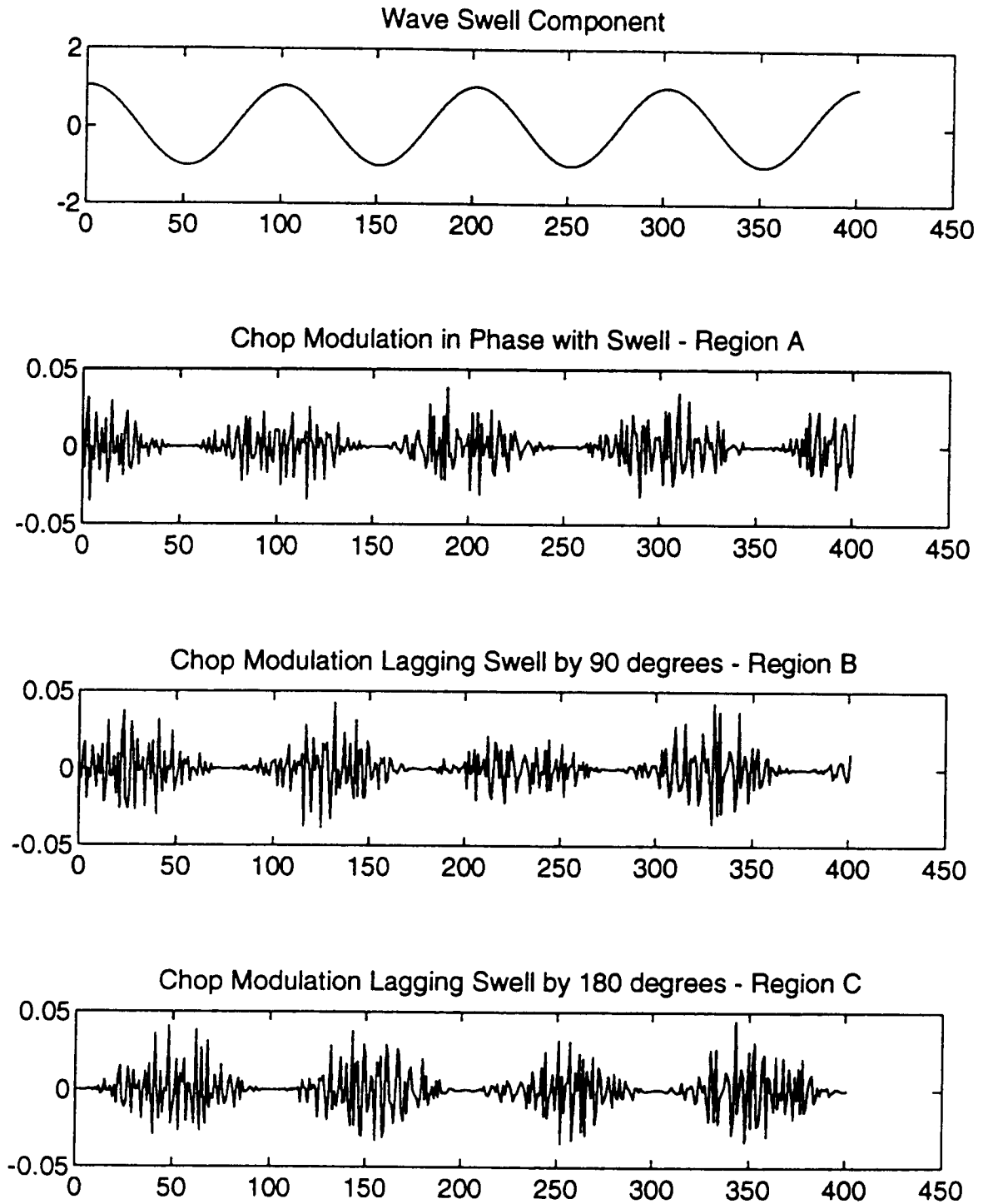


Figure 1-2. Wave Swell vs Chop.  
Test data illustrating the comparison of wave swell component with chop modulation for phase lags of 0 degrees, 90 degrees and 180 degrees.

However, if we now allow for nonlinear interactions between the chop waves, the collective mode theory implies that the chop waves will still respond in a coherent manner to a disturbance such as the swell, but this response is not immediate because the system of chop waves, acting as a medium for the mode, collectively possesses stiffness and inertia; thus it has its own natural frequency of oscillation much like a simple harmonic oscillator.

The natural frequency of the oscillator is given by the dispersion law of Figure 1-1. For example, consider that the wave number of the swell is in region A. The collective mode will respond at the frequency with which it is driven, the frequency of the swell, but its natural frequency is seen to be greater. Thus it tends to respond in phase with the swell, as shown in Figure 1-2(A), like a harmonic oscillator in its stiffness controlled regime. If the wave number should decrease to point B of Figure 1-1, the collective mode is driven at resonance, and like a harmonic oscillator in its dissipation controlled regime, the phase of the chop modulations should lag by  $\pi/2$  as in Figure 1-2(B). In the long wave length limit, region C of Figure 1-1 and Figure 1-2(C), the chop modulations should be out of phase with the swell like an oscillator in its mass controlled regime; just the opposite of the expected result if we neglect the interaction between the waves of the chop.

In order to see evidence of the collective mode, the swell frequency should be well separated from the spectrum of the chop. In much of this thesis we considered the lowest frequency components of the equilibrium distribution to be the "swell" which modulates the higher frequency components, which we called the "chop". Falkovich and Larraza, in private conversation, have since pointed out to us that this may have been an unfortunate choice. The simple oscillator picture is complicated by the possible presence of Landau damping of the collective mode (Larraza, 1993).



However, in a wave tank experiment described below, we were able to control the frequency of the swell and happened to achieve the desired frequency separation. The results from the wave tank experiment are the best evidence of the collective mode.

The techniques and tools developed in this thesis are a method for investigating the relationships between modulations of the chop and phase of the swell in water wave data.

## II. THE DATA

This thesis is primarily about the analysis of field data so most of the effort was directed towards gaining useful information from the one data set obtained. Another data set from the wave tank experiments was also analyzed.

Data set one is a sequence of wave height measurements, WS8714, provided by Dr. Mark A. Donelan of the National Water Research Institute, Canada Centre for Inland Waters, Burlington, Ontario, Canada. The sequence contains 36,000 measurements taken at a 20 Hz sampling rate at a single wave height measurement staff at a site near the southwest end of Lake Ontario, Canada (Donelan, 1985). Figure 2-1 is a power spectrum estimate of the data calculated using a 1024 point FFT and a Hanning window. Empirical studies of the ocean have shown, that for frequencies higher than the spectral peak the power spectrum initially follow an  $\omega^{-4}$  dependence, and at higher frequencies, an  $\omega^{-5}$  dependence (Forristall, 1981). Plotted alongside the power spectrum is a line representing  $\omega^{-4}$ . The power spectrum shows a good fit being slightly shallower for frequencies below 1 Hz and slightly steeper at frequencies above 2 Hz.

Data set two is a sequence of wave height measurements taken in the Ocean Acoustic Wave Facility at the Naval Postgraduate School by Lt. Patricia Gill. The sequence contains 32,768 measurements taken at a 20 Hz sampling rate. A large paddle was used to excite the lowest normal mode of the tank to simulate the swell. The high frequency chop was generated by wind from fans blowing across the surface of the water in the tank. The power spectrum estimate for the tank data is shown in Figure 2-2. For frequencies above 2 Hz, the wind driven waves show a fair fit to the  $\omega^{-4}$  line also plotted for comparison.

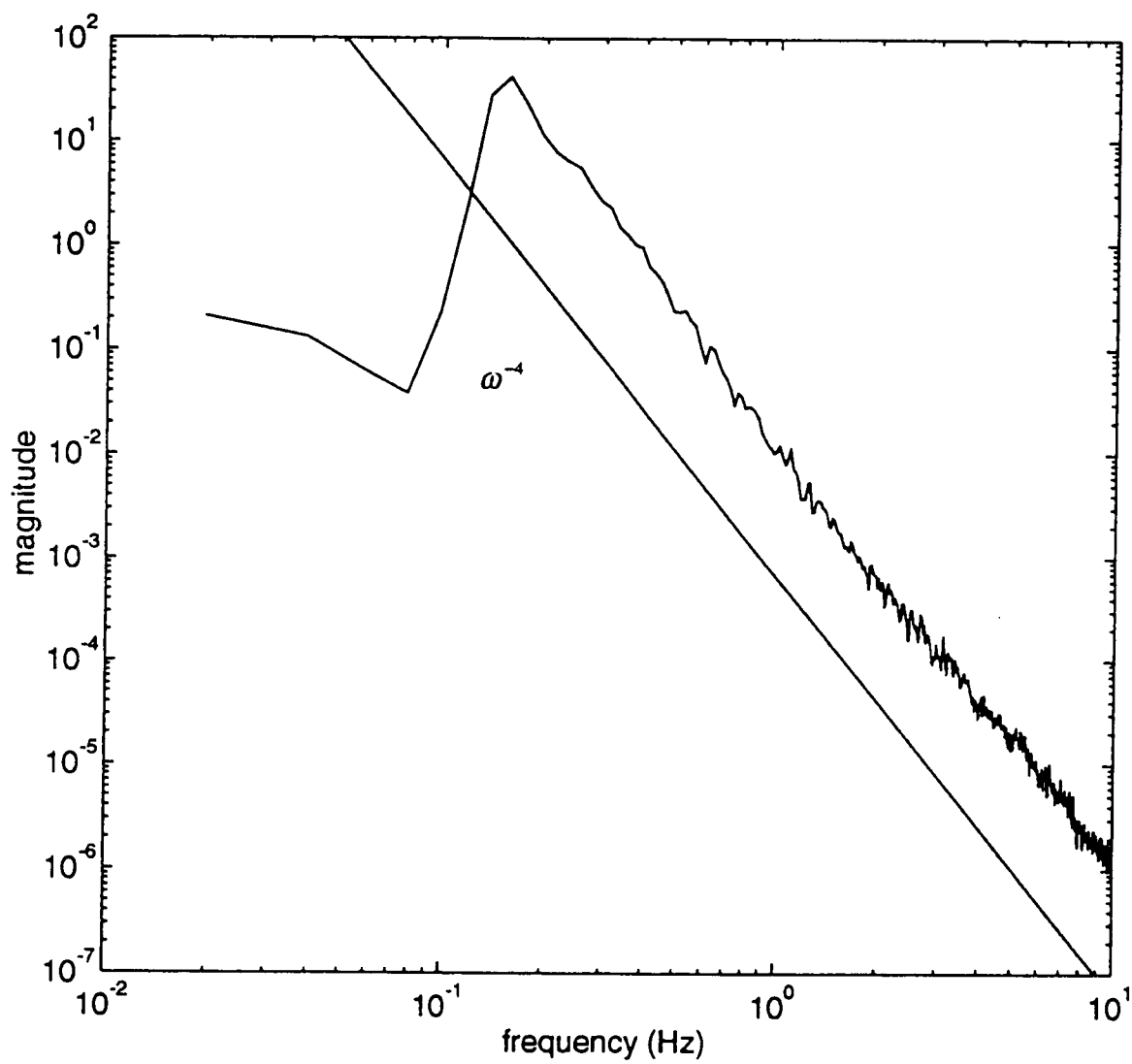


Figure 2-1. Power Spectrum Estimate of Wave Field Data  
Straight line with slope of  $\omega^{-4}$  is plotted for comparison.

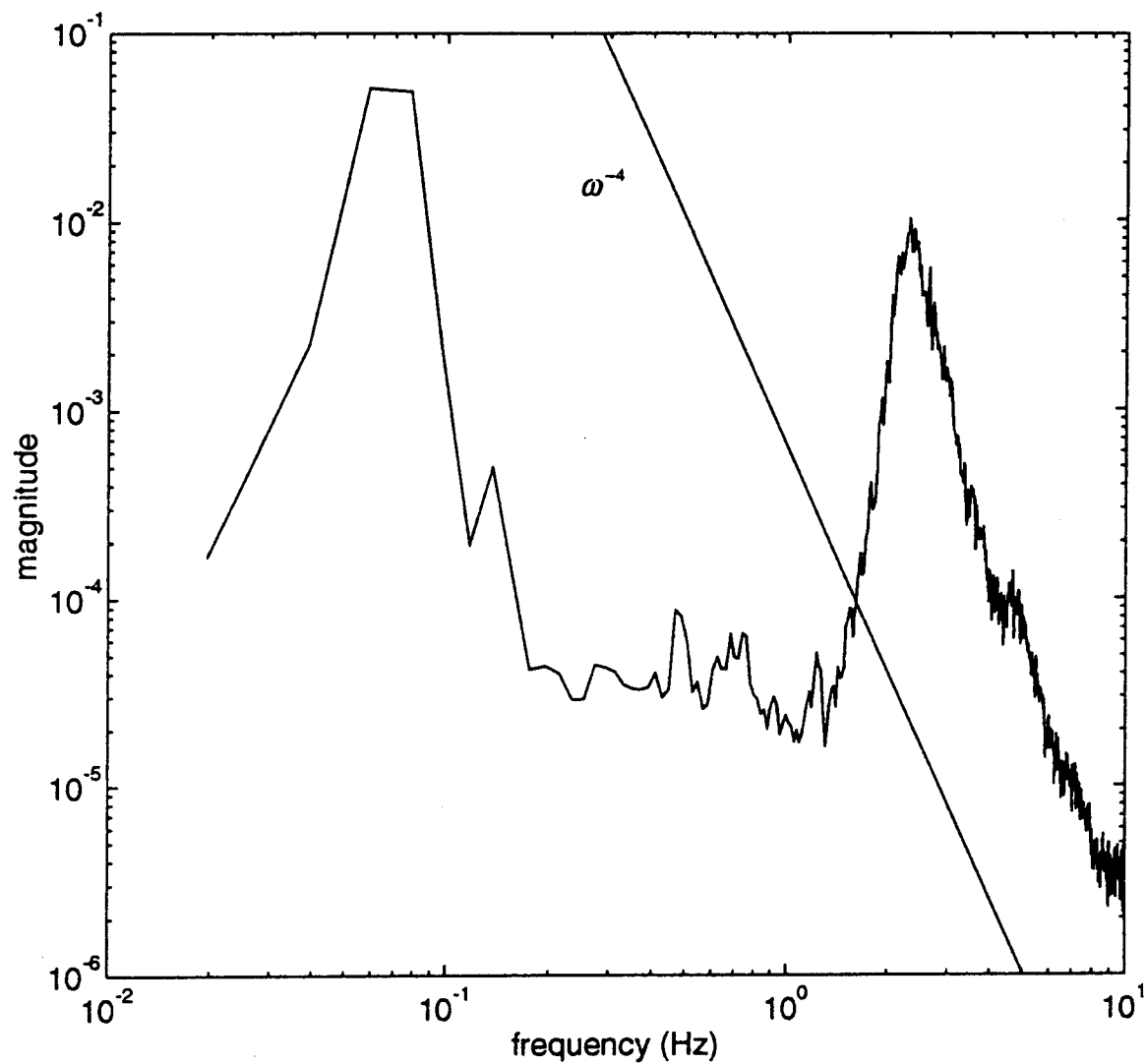


Figure 2-2. Power Spectrum Estimate of Wave Tank Data.  
 The large low frequency peak is the first normal mode frequency of the tank.  
 Straight line with slope of  $\omega^{-4}$  is plotted for comparison with the wind driven chop.



### **III. THE FAST FOURIER TRANSFORM APPROACH**

#### **A. INTRODUCTION**

The first approach employed the Fast Fourier Transform to calculate the power spectra of the sampled wave data. It was thought, that by adjusting the length of the transform to be only a fraction of the period of the swell, and directly examining the frequency components of the chop that occur during this short time, the modulations of the chop power could hopefully be found to have a preferred phase relation with respect to the swell.

#### **B. PROCEDURE**

The analysis program takes a data sample of length  $2^n$ , applies a Hanning window to it and then computes the power spectrum of the sample. At the same time, the average of the sample is calculated to obtain an estimate of the instantaneous swell height. The process is repeated with each sequential sample until all of the data file has been processed. The power spectra are stored in a two dimensional matrix whose rows are frequencies and whose columns are time intervals. Entries in the matrix are power levels in units of dB/10. The swell height values are stored in another array. The power spectra are presented on a frequency versus time plot with the vertical axis being frequency and the horizontal axis being time. The power level at a given frequency and time is represented by gray shading. Higher power levels are dark gray and progressively lighter shades are lower power levels.

The modulations of the chop power over time should appear as alternating dark and light vertical bands. The average height information is presented on a two dimensional plot.

Additional processing to permit a rough determination of the phase is made by sorting the average height measurements into four categories: (1) rising slope, (2) peak, (3) falling slope, and (4) trough. The power level in each of the higher frequencies (chop) is plotted against the average wave height (swell) for each of the categories on four separate scatter diagrams. The mean chop power level and mean swell height in each category are calculated for each frequency. Histograms of the distribution of power levels in each category are also plotted.

### **C. OBSERVATIONS**

Rather than the energy being distributed completely at random, the alternating light and dark vertical bands of energy in Figure 3-1 show that modulations of the chop do indeed occur. Contours are also plotted to highlight the regions of higher energy.

When dealing with FFTs and windowing of data, there is a concern that 'leakage' from higher energy frequencies may be showing up in other lower energy frequency bins. Since the power spectrum of this data shows much higher power levels are present in the lower or swell frequencies, it could be the case that what we are seeing is a processing artifact of the windowing rather than true modulations of the chop. Figure 3-2 compares the power spectra of a dark band and its adjacent lighter bands to the magnitude-frequency response of the Hanning window centered on a frequency of 0 Hz. The power levels at the high frequencies in the dark band are noticeably greater than could be attributed to leakage of the Hanning window thus supporting the contention that compressions of the high frequencies are occurring.

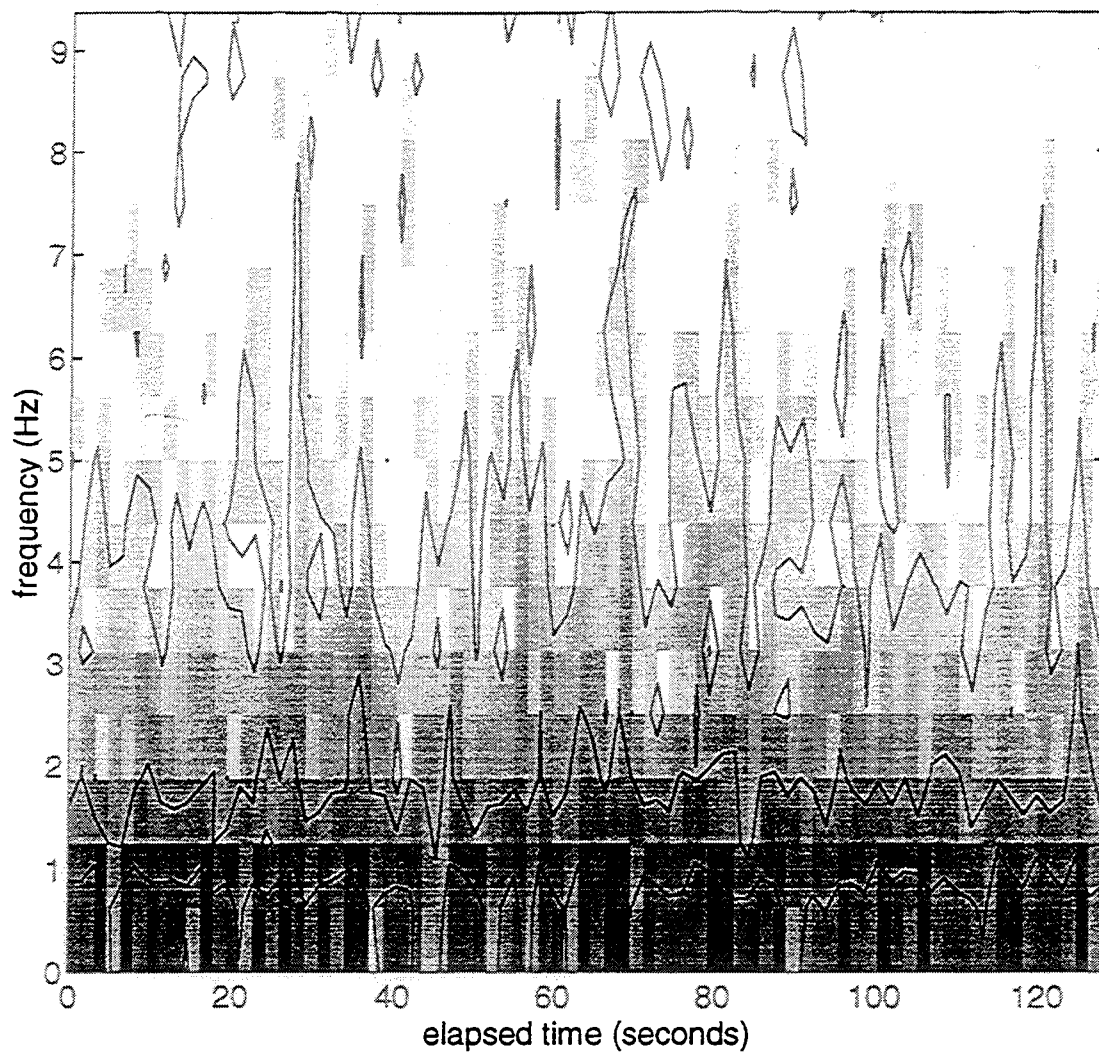


Figure 3-1. Example Frequency-Time Plot of Portion of Wave Field Data  
Alternating vertical bands of dark (higher energy) and light (lower energy) indicate modulation of the higher chop frequencies.



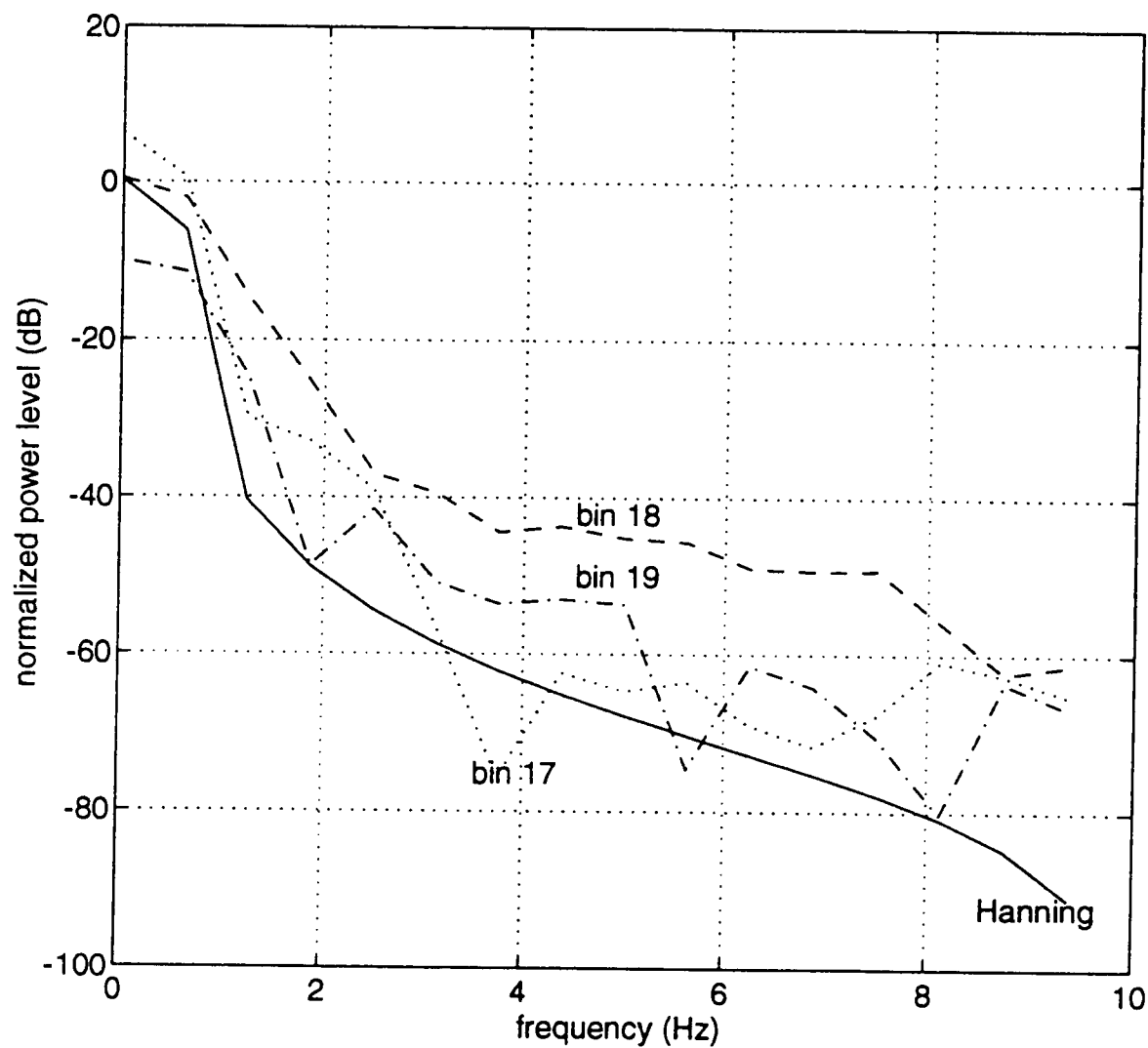


Figure 3-2. Comparison of Time Bin Power Spectra Vs Hanning Window  
 Time bin 18 (dashed line) is a dark band; bins 17 (dotted line) and 19 (dash dot line) are the adjacent light bands. Leakage of a Hanning window centered on frequency = 0 Hz is shown with the solid line.

To answer the question of when in the phase of the swell these compressions of the chop are taking place, the following two step method was used. The first step was to increase the time resolution by shortening the length of the sample over which the power spectrum was being calculated to be some fraction of the period of the swell. The swell frequency was assumed to be in the lowest frequency bin of the spectrum. This had the detrimental effect of reducing the overall frequency resolution. The problem was that the size of the individual frequency bins spanned across both the swell and chop frequencies so that power in the lower swell frequencies overwhelmed the subtle changes in the compressions/expansions of the higher chop frequencies. In the plots and analysis presented here a sample length of 32 points was used. This sample length provided an acceptable compromise between frequency resolution and time resolution for the analysis which follows. The second step in our method for determining the phase of the swell was to calculate the average height of the wave data over the sample length. The resultant smoothed signal approximated the swell frequencies.

Figure 3-3 shows the average height of the wave plotted over the same time period as the frequency spectra. The frequency versus time plot from figure 3-1 is repeated here to allow visual comparison of the average heights with their corresponding power spectra. Each point on the lower plot (marked with +) represents the average height of the wave within a 32 point sample or time bin. Each time bin is one vertical band in the upper plot.

To further aid in the comparison of the amplitude of the chop frequencies with the phase of the swell frequencies additional processing to permit a rough determination of the phase is made by comparing each average height measurement with its two nearest neighbors, and sorting them into four phase categories: (1) rising slope, (2) peak, (3) falling slope, and (4) trough.

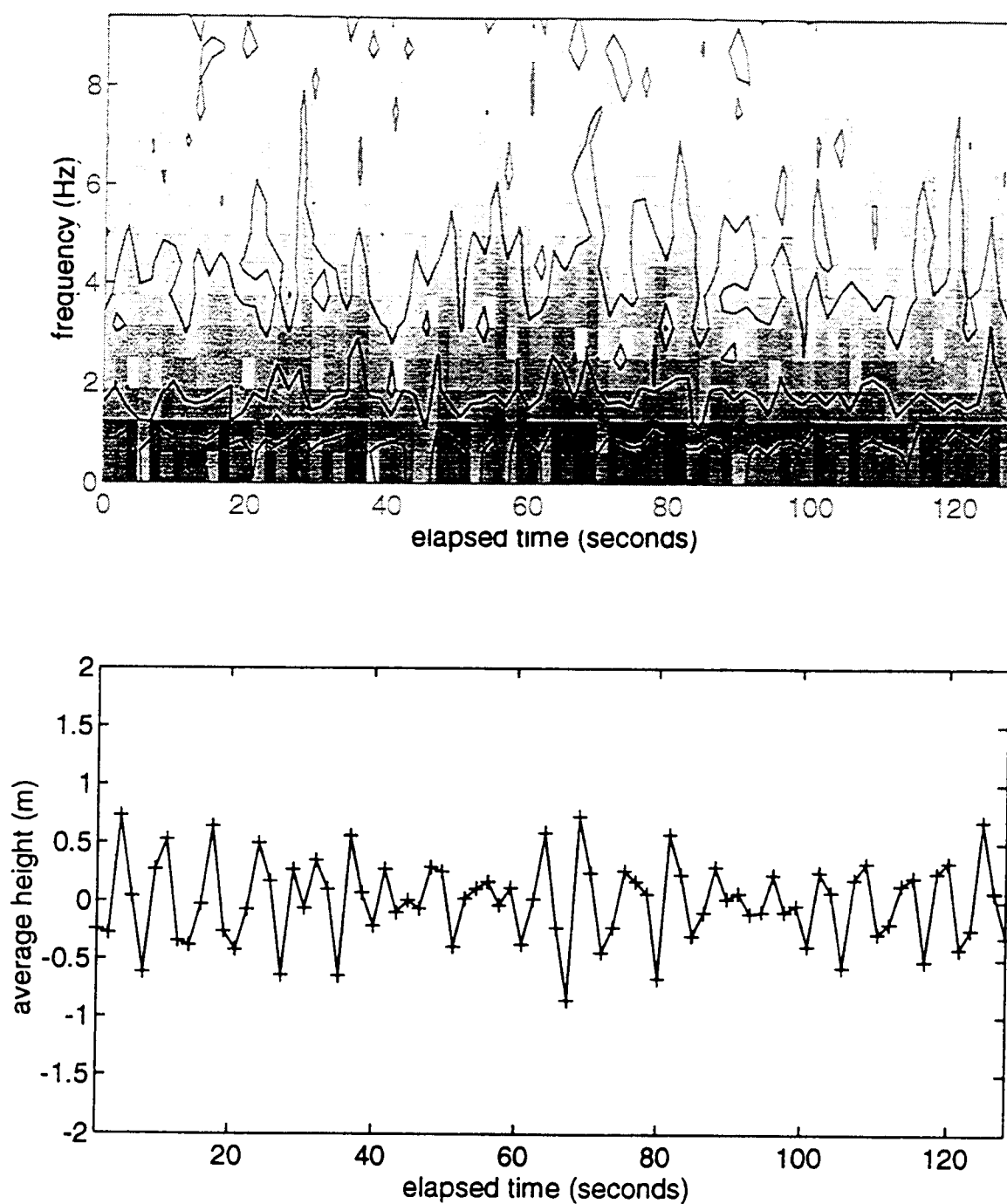


Figure 3-3. Example Frequency-Time Plot and Average Height Plot  
Each point on the lower plot (marked with +) represents the average height of the wave within a 32 point sample or time bin. Each time bin is one vertical band in the upper plot.

Figure 3-4 is an example of four scatter diagrams of the power levels versus average height for frequency bin number 3; center frequency 1.875 Hz. These are typical of the scatter diagrams produced for frequency bins 3 through 16 covering frequencies from approximately 1.5 Hz to 10 Hz.

As expected, the mean swell height is highest for the peaks, lowest in the troughs and near zero for the rising and falling slopes. Examination of the mean chop power levels in each phase category reveals that the highest power levels and therefore the greatest compressions occur near the peaks of the swell. This is indicative of a zero phase shift between the amplitude modulations of the chop and the phase of the swell. The distribution histograms of each category were examined to see if there was any visible skewing in the distribution. All of the histograms showed that within each category the power level distribution closely matched a Normal or Gaussian distribution with no skewing.

Figure 3-5 shows the distribution histograms for frequency bin 3 which are typical of all of the frequency bins.

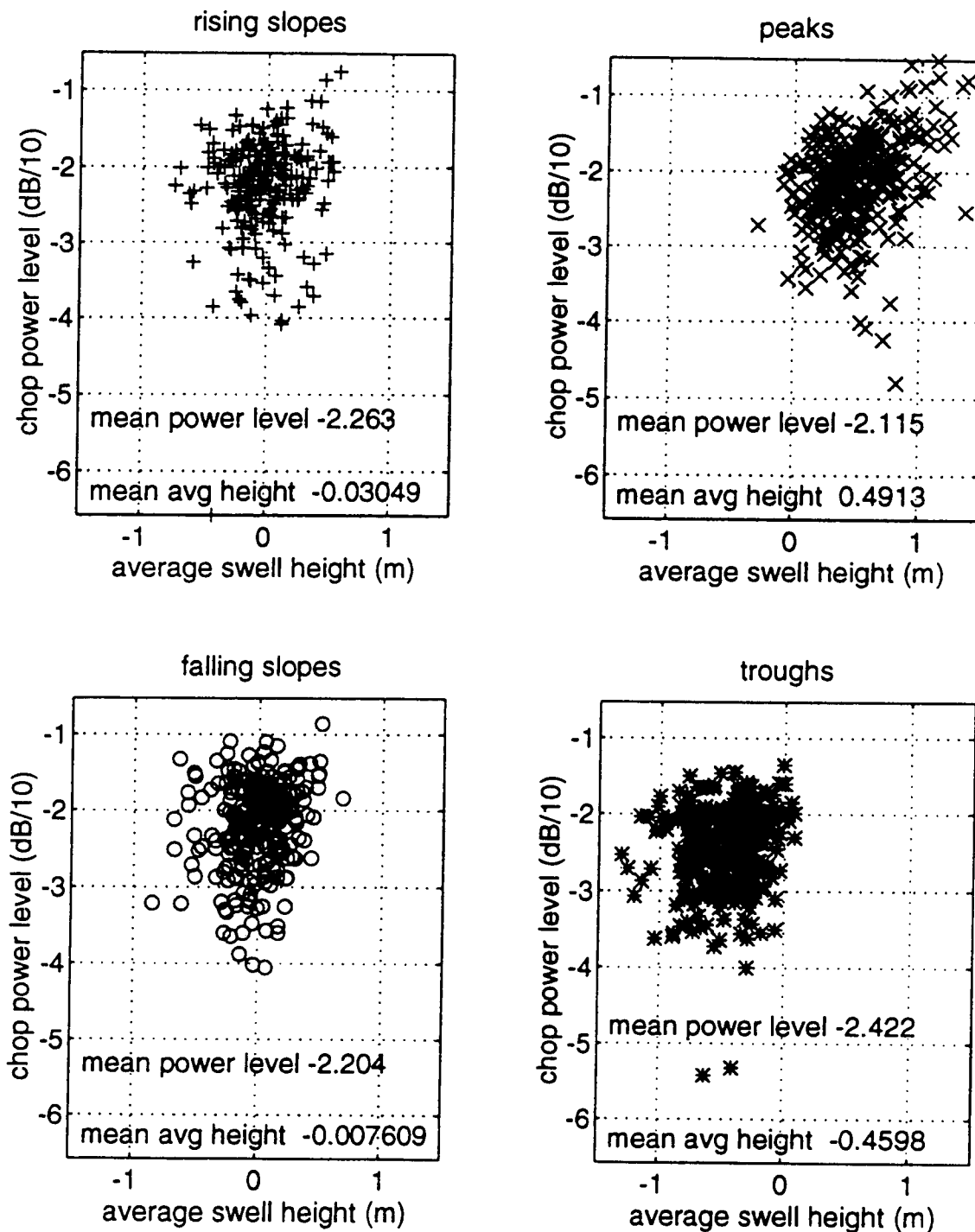


Figure 3-4. Scatter Diagrams for Frequency Bin 3. Center Frequency 1.875 Hz.  
 Note: The highest mean chop power levels are occurring at the peaks of the swell.

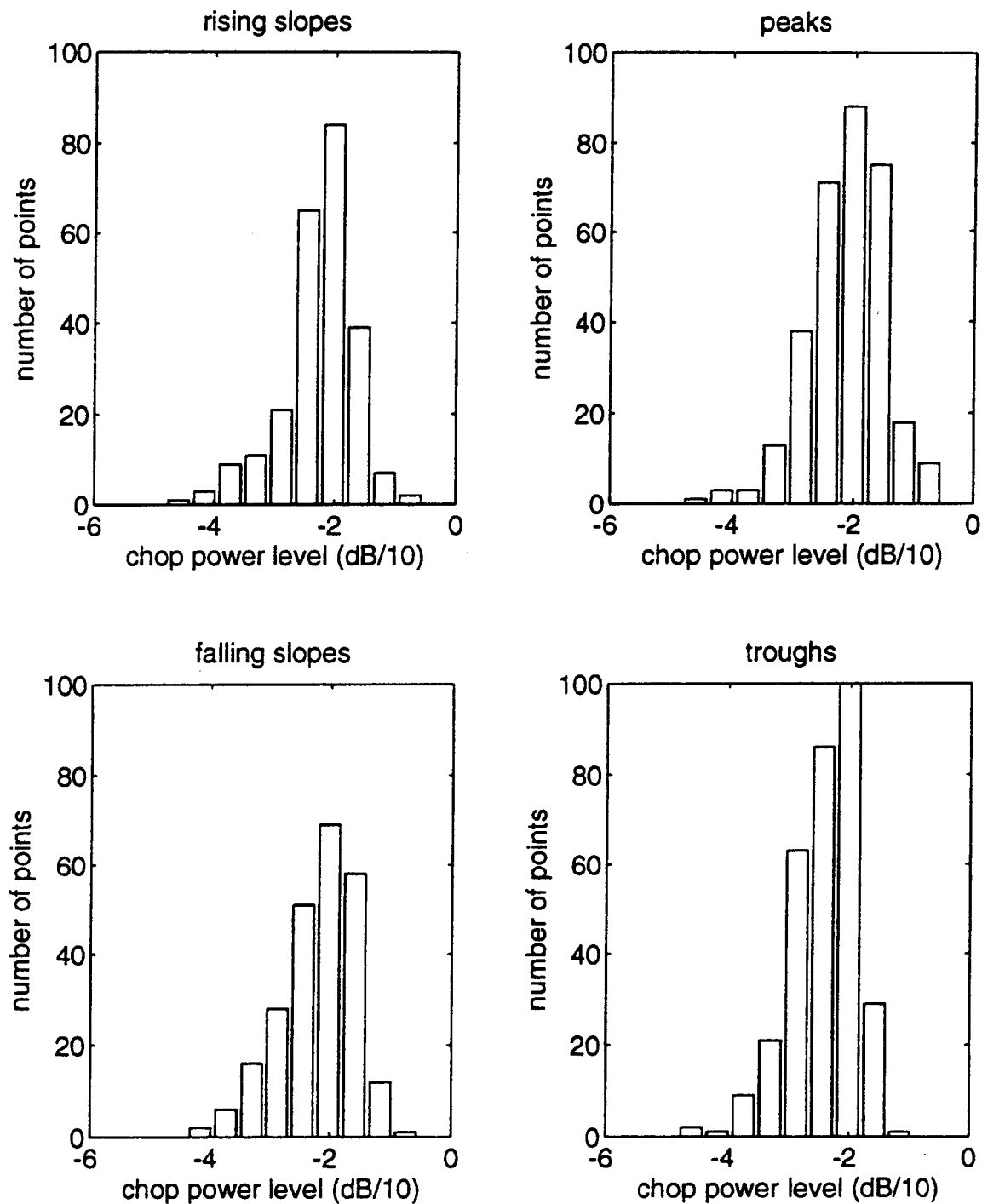


Figure 3-5. Chop Power Level Distribution Histograms for Frequency Bin 3.  
 Note: None of the distributions show any marked skewing. These are typical of the distributions for all of the frequency bins.



## **IV. THE HILBERT TRANSFORM APPROACH**

### **A. INTRODUCTION**

The FFT approach did not concurrently provide adequate resolution in the time and frequency domains to permit direct comparison of the phase of the lower swell frequencies with the modulations of the amplitude of the higher chop frequencies. To overcome this it was decided to employ the Hilbert Transform from which the instantaneous amplitude (compressions) and the instantaneous phase could be computed directly. The Hilbert Transform also has the desirable property that the transformed signal remains in the same domain as the original signal allowing one to work exclusively in the time domain. To properly employ this tool it was necessary to separate the high and low frequencies using the techniques of digital signal processing. Care had to be taken not to corrupt either the phase or amplitude information of the original wave data.

### **B. BACKGROUND**

#### **1. The Hilbert Transform**

The Hilbert Transform of a real-valued time signal is a complex signal called the analytic signal. The real part of the analytic signal  $x$  is the original real-valued time signal while the imaginary part  $y$  is a copy of the original signal with each of its Fourier components shifted in phase by  $90^\circ$  (Haykin, 1983). The transformed signal retains the



same amplitude and frequency content as the original and also includes phase information dependent on the phase of the original data.

The instantaneous amplitude of the original signal is obtained by calculating the amplitude of the analytic signal:

$$hilbert\_amplitude = \sqrt{x^2 + y^2} . \quad \text{IV.B.1}$$

The instantaneous phase of the original signal is similarly obtained by calculating the phase of the analytic signal:

$$hilbert\_phase = \arctan\left(\frac{y}{x}\right). \quad \text{IV.B.2}$$

Each of the calculated amplitude and phase values is highly localized spanning approximately three to four of the original signal data points.

The Matlab function *hilbert* (Mathworks, 1993) approximates the analytic signal with a different but equivalent approach. It first calculates the FFT of the original input sequence. The FFT coefficients that correspond to negative frequencies are set to zero and then the inverse FFT of the sequence is calculated. The result is the complex valued analytic signal.

## 2. The Chebyshev Type II Filter

The selection of the appropriate filter used to separate the low frequency 'swell' from the high frequency 'chop' was governed by the desired characteristics of the resulting filtered signal. The filter could not introduce phase distortion, it had to maintain amplitude information in the pass band while minimizing the distortion of the small amplitude fluctuations, the stop band had to be at least 40 dB below the pass band to eliminate possible leakage problems and it had to have a minimum transition width to ensure good

frequency separation. Also because higher order filters could introduce numerical errors, the filter had to meet the requirements with the lowest order filter possible.

The Matlab Signal Processing Toolbox (Mathworks, 1993) offers two techniques for the design of digital filters (1) Direct Design and (2) Analog Prototyping. The Direct Design technique, while offering precise control over the filter characteristics, consistently produced filters which were of such a high order as to raise concerns about numerical accuracy. Both Finite-duration Impulse Response (FIR) and Infinite-duration Impulse Response (IIR) filters were designed using this technique with similar results.

The Analog Prototyping technique allows the construction of digital equivalents of certain classical analog filters, specifically the Butterworth, Bessel, Chebyshev, and Elliptic. The Butterworth filter has a wide transition, being maximally flat in the pass band and the stop band and smoothly decreasing in between. The Bessel filter also has a wide transition, and when mapped into a digital equivalent is not maximally flat in the pass band, thereby introducing distortion in the small amplitude fluctuations. The Chebyshev Type II filter has a narrower transition than for the Butterworth filter, and also has a maximally flat pass band response. The Elliptic filter minimizes transition width, has equiripple in both the pass band and stop band, and generally meets filter specifications with the lowest order of any of the filters supported by Matlab.

Both the Chebyshev Type II and Elliptic filters met the criteria established and produced similar results when applied to the data. For the following analyses the Chebyshev Type II filter was employed.

Analog filters are IIR type filters, and IIR filters necessarily introduce phase distortion. To overcome this problem the wave data was filtered in both the forward and reverse directions by using the Matlab function *filtfilt*. (Mathworks, 1993). The result is precisely zero-phase distortion and doubling of the filter order. In addition, *filtfilt* minimizes startup and ending transients by adjusting initial conditions.

## C. PROCEDURE

### 1. Filtering

The low swell frequencies were isolated by first filtering the data using a low pass Chebyshev Type II filter having the following characteristics: filter order 5, stop band attenuation 40 dB, and cutoff frequency 0.625 Hz.

Similarly the higher swell frequencies were isolated by filtering the data using a high pass Chebyshev Type II filter with the same order and stop band attenuation but with a cutoff frequency of 1.5 Hz. The cutoff frequencies and the level of stop band attenuation were chosen based upon observation of the frequency content and the relative power levels of the data as presented in the power spectrum. The filter order was kept low in order to avoid the possibility of introducing numerical computation errors. As a result of using the two pass *filtfilt* procedure, the actual effective filter order was 10. The sensitivity of the final results to the selection of the above parameter values was tested by varying each parameter individually; no significant differences were observed. Figure 4-1 shows the frequency responses of the low pass and high pass filters used in the first part of this analysis

The selection of the above cutoff frequencies for the swell and chop were based upon what was achievable using the FFT. Digital signal filtering allows much more precise control of the frequencies used in the analysis. Thus, the study of possible dependence relations was later expanded by filtering the data into octave bands using band pass filters. This permitted investigation of relationships between adjacent and next adjacent bands as well as non-adjacent bands.

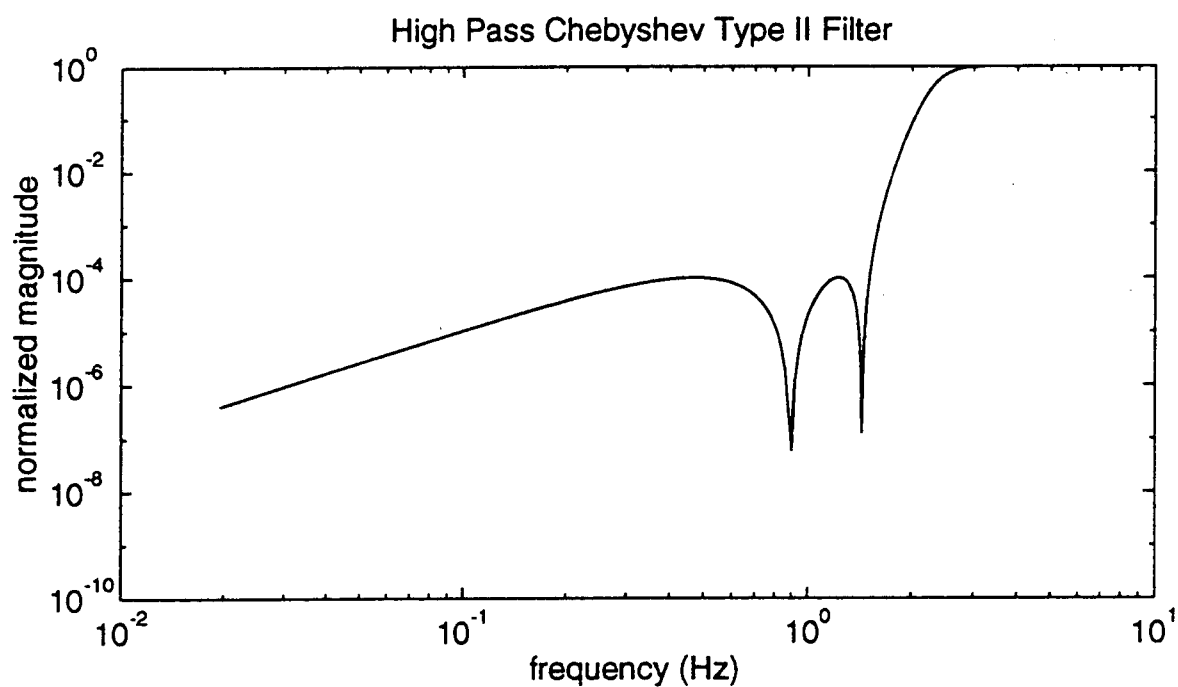
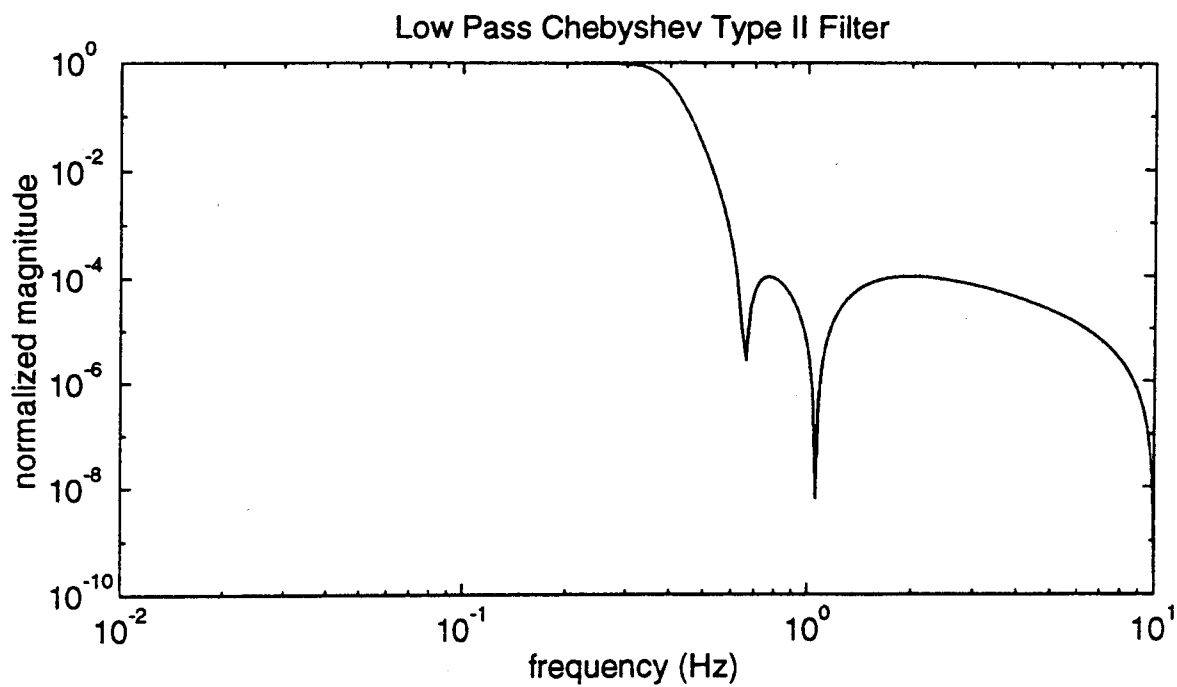


Figure 4-1. Magnitude-Frequency Response of Chebyshev Type II Filters  
 Filter Order -Nominal 5, Effective 10; Stop Band Attenuation 40 dB;  
 Low Pass Cutoff Frequency 0.625 Hz; High Pass Cutoff Frequency 1.5 Hz.

## **2. Instantaneous Phase - Low Wave**

The phase of the low frequency swell is obtained in two steps. First, the Hilbert transform of the output of the low pass filter (or low band) is taken. Second, the phase of the transform is calculated using the function *angle* (Mathworks, 1992) which returns phase angles in radians between  $-\pi$  and  $+\pi$ .

## **3. Instantaneous Amplitude - High Wave**

The amplitude of the high frequency chop is also obtained in two steps. First, the Hilbert transform of the output of the high pass filter (or high band) is taken. Second, the amplitude is calculated using the function *abs* (Mathworks, 1992) which returns the amplitude in length units.

## **4. Plotting**

The amplitude of the high frequency chop was initially plotted against the phase of the low frequency swell on a simple scatter diagram. The scatter diagram provided some useful information, but proved difficult to interpret because of the large numbers of points falling within the lower regions of the diagram.

In order to overcome this problem with the scatter diagram, data points are sorted into a 100 by 100 matrix to determine their distribution. Each row of the matrix represents 1/100th of the amplitude range and each column represents 1/100th of the phase range. Each pair of amplitude and phase values is compared to scales to determine which cell of the matrix should be incremented. The elements of the matrix thus represent the number of

points which would occupy a small region of the scatter diagram. The matrix is plotted with the vertical axis being amplitude of the chop, the horizontal axis being phase of the swell and gray or color shading indicating the density of points. The plots are created interactively using the program Transform (Spyglass, 1993). The rms amplitude of the chop is also calculated from the sorted data and plotted on the same plot.

## 5. Test Signal

To aid in the interpretation of the plotted results of the field data, a test signal was designed which would allow direct manipulation of relevant parameters. The equation of the test signal is

$$test = \cos(2\pi f_{swell}t) + Ar(1 + \cos(2\pi f_{swell}t - \phi)). \quad \text{IV.C.1}$$

List of Variable Parameters and Presets:

1.  $f_{swell}$  - swell frequency 0.2 Hz
2.  $A$  - constant high frequency amplitude multiplier 0.04
3.  $r$  - random high frequency amplitude multiplier uniform random value [0,1]
4.  $\phi$  - phase shift angle in radians  $\left[0, \frac{\pi}{2}, -\frac{\pi}{2}, \pi\right]$

Figure 4-2 shows three signals; the original Test Signal with a zero phase shift between the chop and the phase of the swell, the result after low pass filtering which is called the swell, and the result after high pass filtering which is termed the chop.

Figure 4-3 shows the low frequency wave or swell component of the test signal and the phase of the swell as output by the Hilbert transform. Observe that phase values at the extremes (i.e.  $-\pi$  and  $+\pi$ ) represent the troughs of the waves, while phase values of zero represent the crests of the waves. This standard interpretation of the phase values is used throughout this analysis.

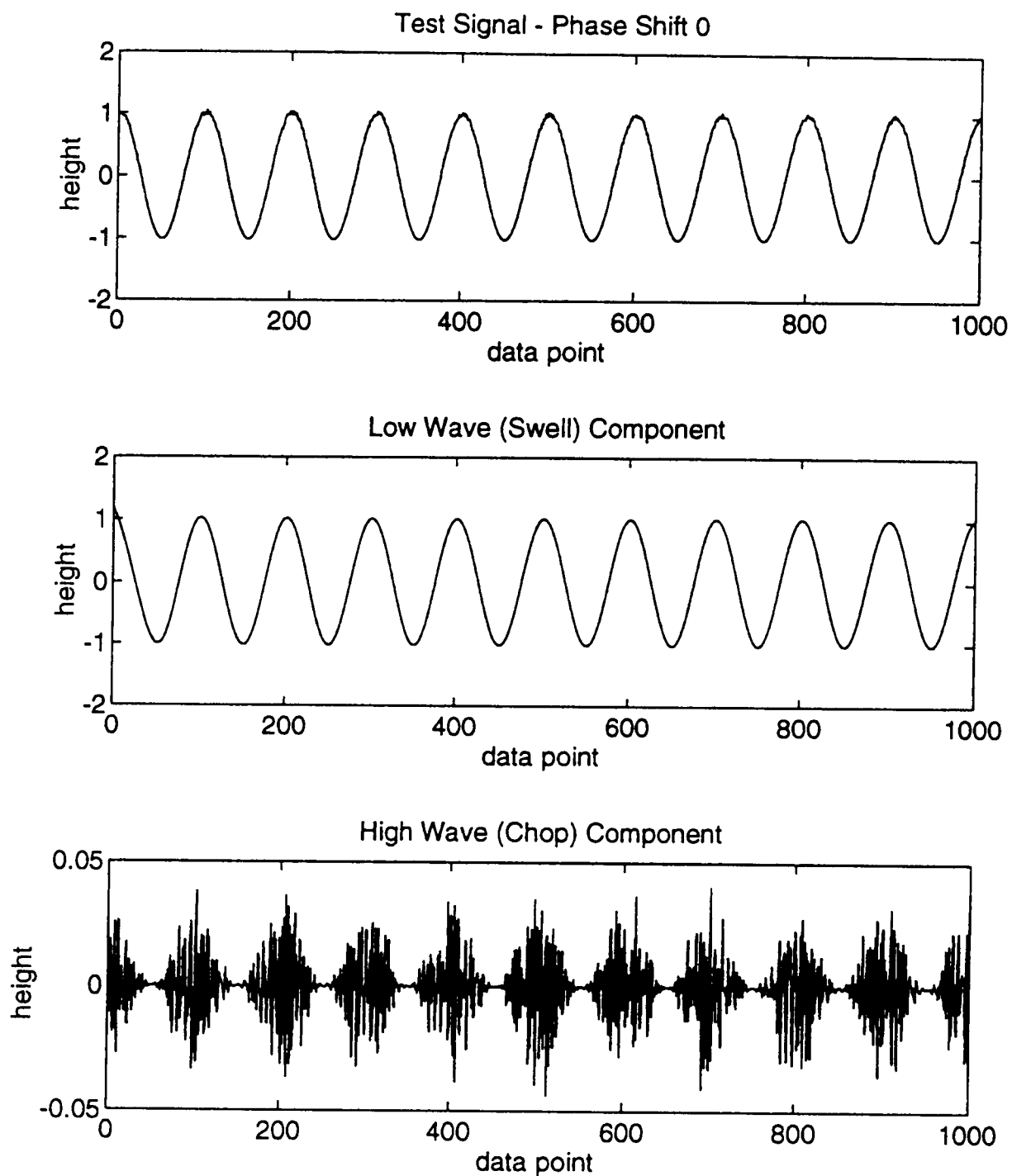


Figure 4-2. Test Signal , Low Wave (Swell), and High Wave (Chop)  
Phase shift of Test Signal is 0 degrees.

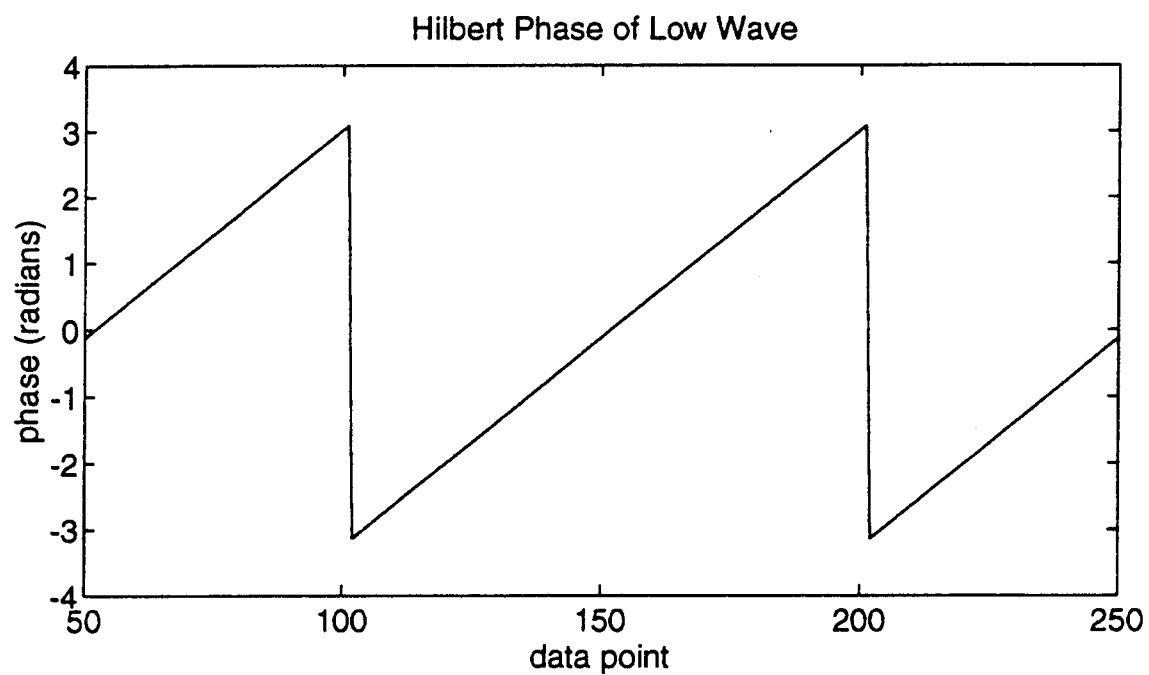
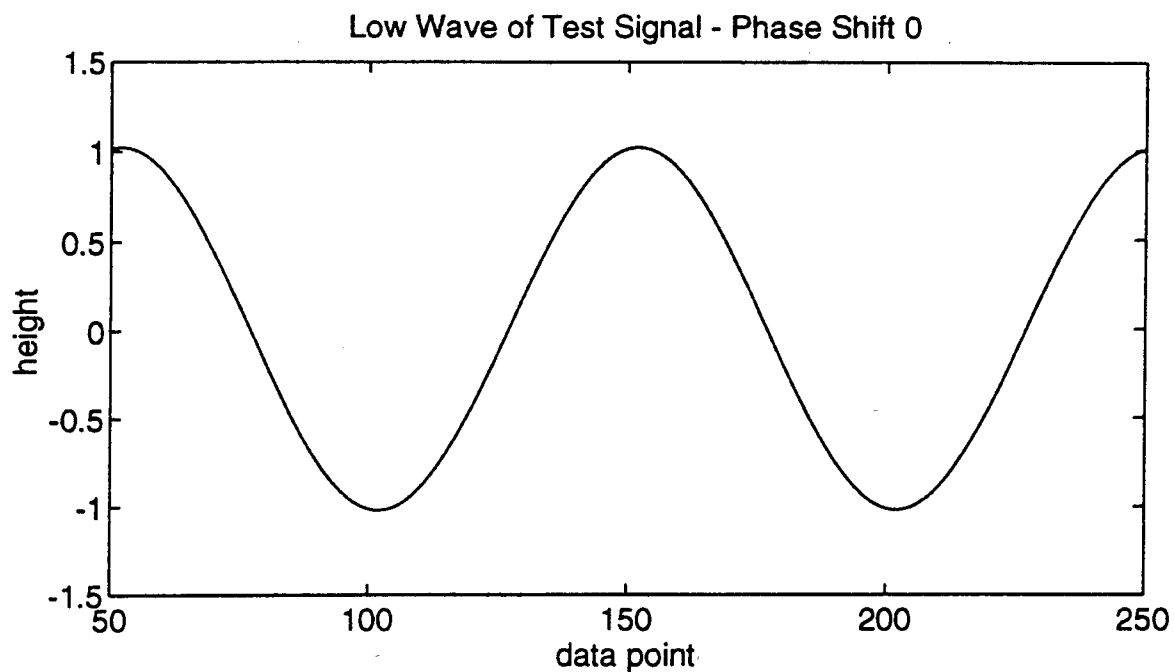


Figure 4-3. Swell Component of Test Signal and Hilbert Phase of Swell  
Observe that phase values at the extremes (i.e.  $-\pi$  and  $+\pi$ ) represent the troughs of the waves, while phase values of zero represent the crests of the waves.



Figure 4-4 shows the high frequency waves or chop component of the test signal and the amplitude of the chop as output by the Hilbert transform. Comparing Figure 4-4 with the previous Figure 4-3, observe that the greatest amplitude values are occurring at the peaks of the low wave as is expected with zero phase shift.

Figure 4-5 shows a portion of each of four test signals with phase shifts of  $0^\circ$  (crest),  $+90^\circ$  (falling slope),  $-90^\circ$  (rising slope) and  $180^\circ$  (trough). Figure 4-6 shows the resulting amplitude versus phase distribution plots of the signals on Figure 4-5. The solid line on the plots represents the rms average of the chop amplitude at each phase of the swell. The distribution plots on Figure 4-6 illustrate the characteristic shapes and shadings that correspond to the different phase shift relationships between the swell and the chop that we seek in the field data.

## **D. OBSERVATIONS**

### **1. Filtering - Wave Field Data**

The same low pass and high pass Chebyshev Type II filters developed for use with the test signals were used to filter the wave field data and later with minor modifications were also used to filter the wave tank data. The low pass cutoff frequency for the wave field data was set at 0.625 Hz. The high pass cutoff frequency was set to 1.5 Hz. These were the same cutoff frequencies used with the test signals. Again, the sensitivity of the final results to the selection of the filter parameters was tested by varying the values. No significant differences were observed.

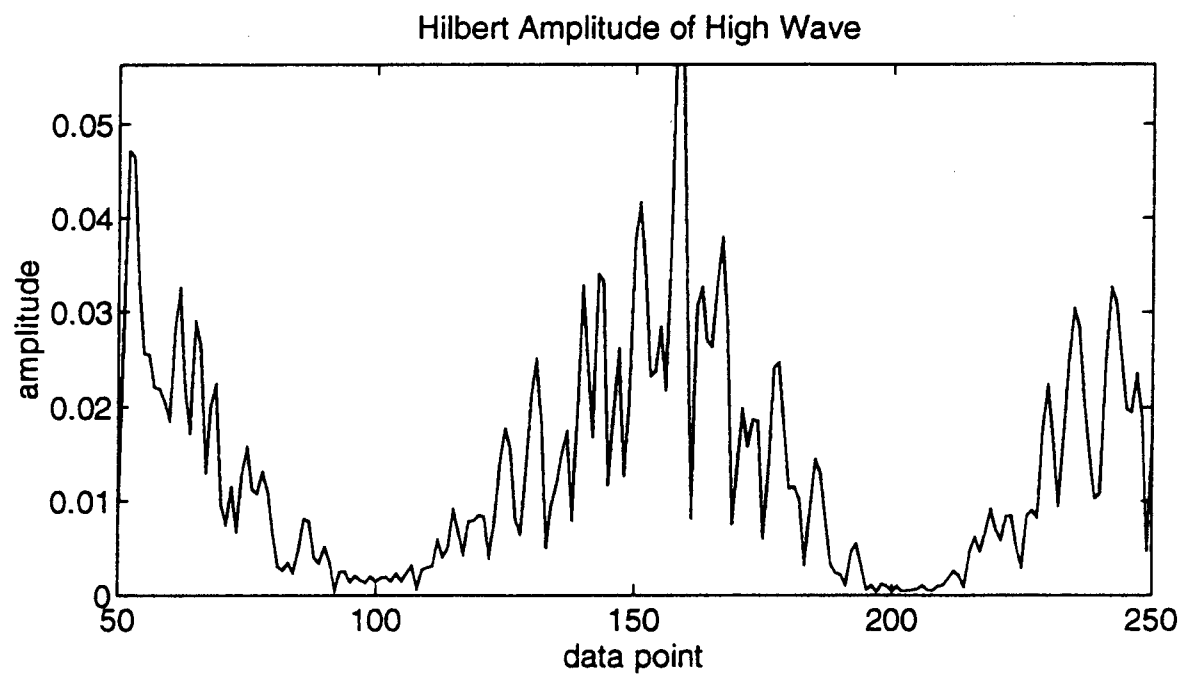
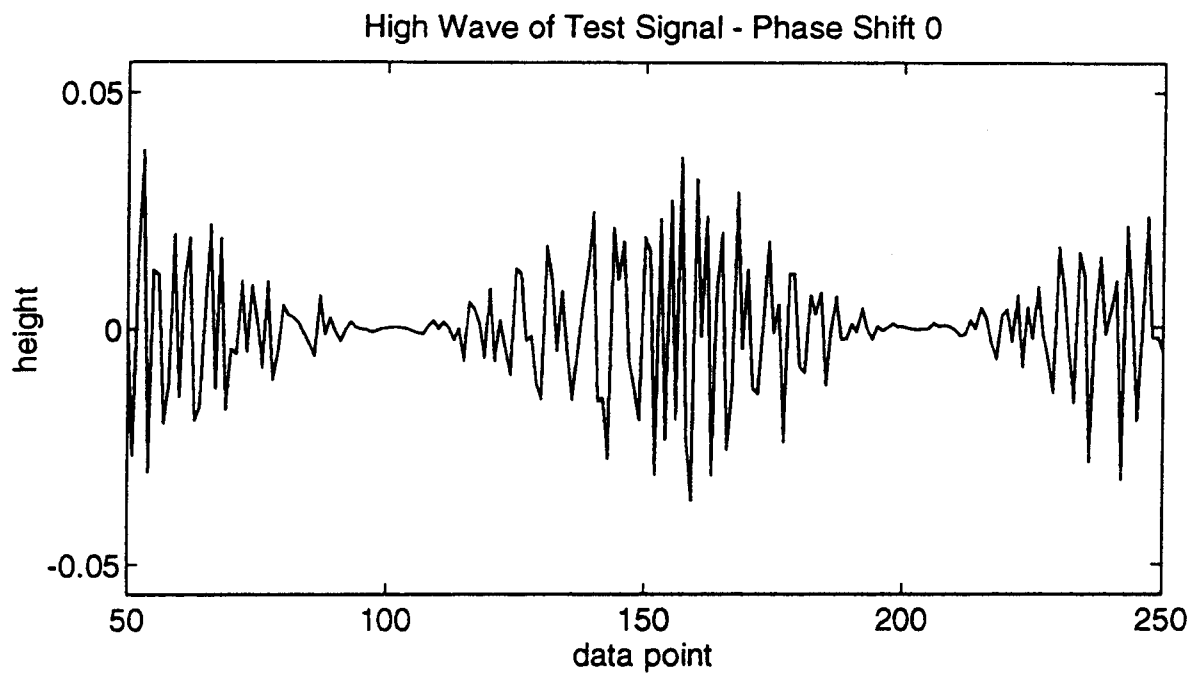


Figure 4-4. Chop Component of Test Signal and Hilbert Amplitude of Chop

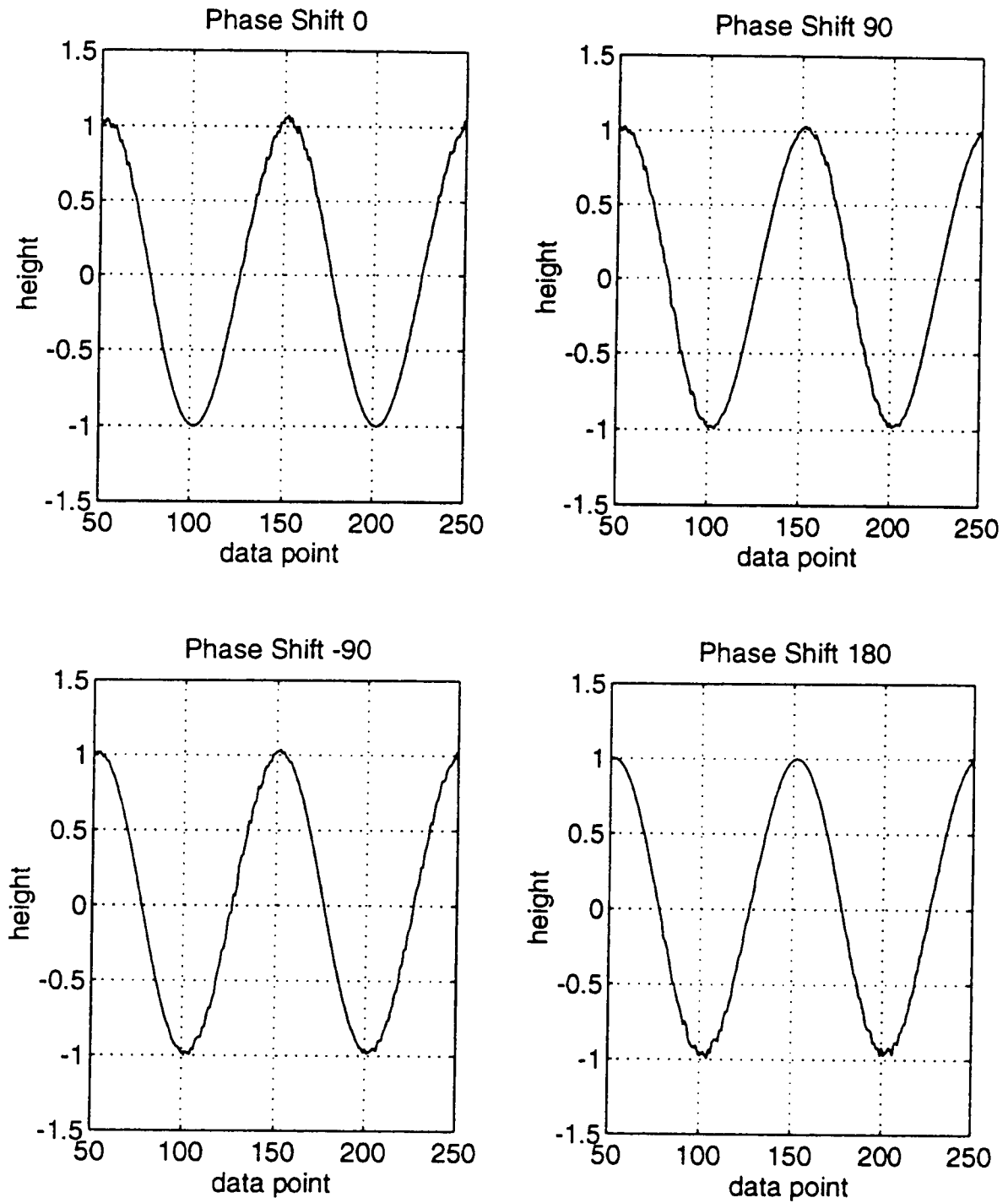


Figure 4-5. Test Signals - Phase Shifts 0, 90, -90, and 180 Degrees

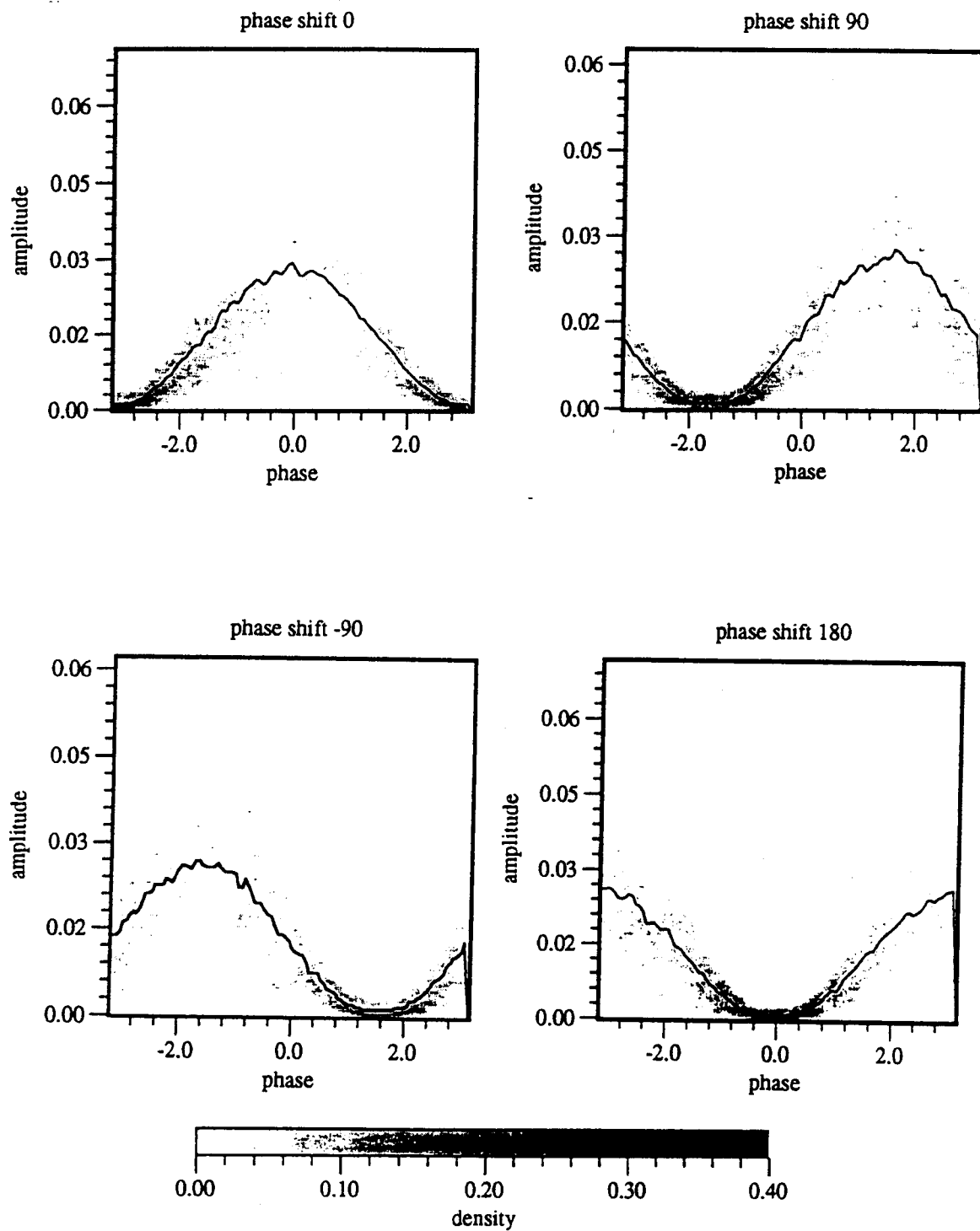


Figure 4-6. Distribution Plots of Amplitude of Chop vs Phase of Swell for Test Signals - Phase Shifts 0, 90, -90, and 180 degrees. Solid line is rms average of the Chop Amplitude.

Figure 4-7 shows the first 1000 points of the original wave field data, the low wave or swell component output from the low pass filter, and the high wave or chop component output from the high pass filter. Figure 4-8 shows the power spectra of these three waves and illustrates how they relate to each other in the frequency domain.

## **2. Scatter Diagram - Wave Field Data**

The amplitude of the chop and the phase of the swell are each calculated as described in the procedure above. Figure 4-9 is a scatter diagram of the amplitude versus phase values. The plot contains 36,000 data points, most of which are plotted in the lower amplitude range from 0 to 0.015. Only a few thousand points are plotted in the amplitude range from 0.015 to 0.11. The central mass of these points is slightly to the right of zero phase possibly indicating that the maximum compressions of the chop lag slightly behind the crest of the swell. This was initially an exciting result because it supported the wave turbulence collective mode picture. However, it was noticed that these were rare, relatively high chop amplitude, events.

To determine what was different about these points, the information was subdivided into successively smaller samples until it became possible to associate particular groupings of amplitude versus phase points with their corresponding data points in the original wave data. Figure 4-10 illustrates two of these groupings and shows where they fall in the original wave data. Event one from data point 4860 to 4880 occurs on the trailing side of a wave whose crest has just passed the wave height staff. Event two from data point 4920 to 4950 occurs on the leading edge of a wave whose crest has not yet reached the staff.

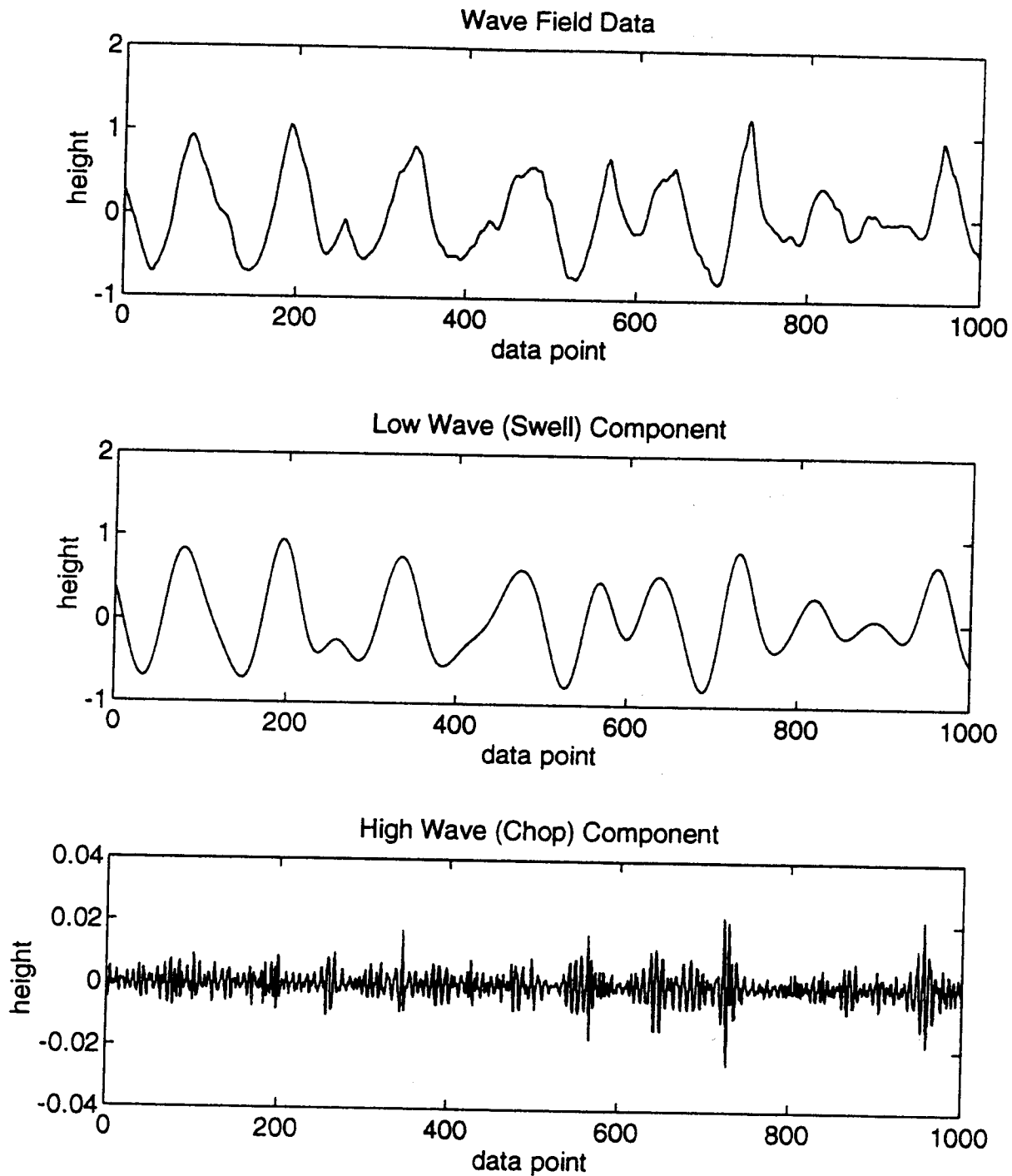


Figure 4-7. Wave Field Data, Low Wave (Swell), and High Wave (Chop) Swell is output of Low Pass Chebyshev Type II filter. Chop is output of High Pass Chebyshev Type II filter. Only the first 1000 points of each sequence are plotted.

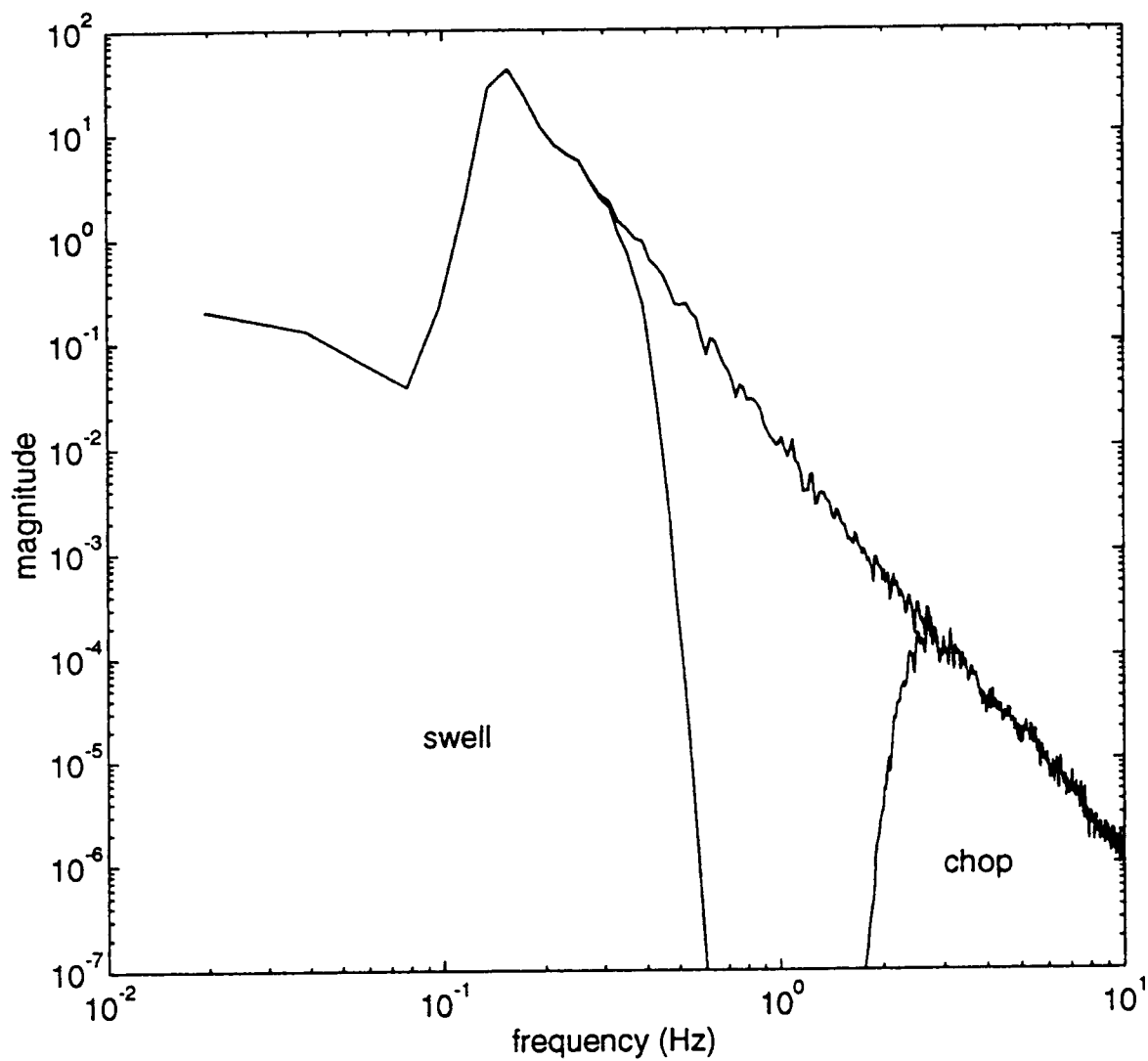


Figure 4-8. Power Spectra of Wave Field Data, Swell and Chop  
 Location of the swell and chop components of the field data are indicated by their respective power spectra. Cutoff frequency for the swell is 0.625 Hz. Cutoff frequency for the chop is 1.5 Hz.

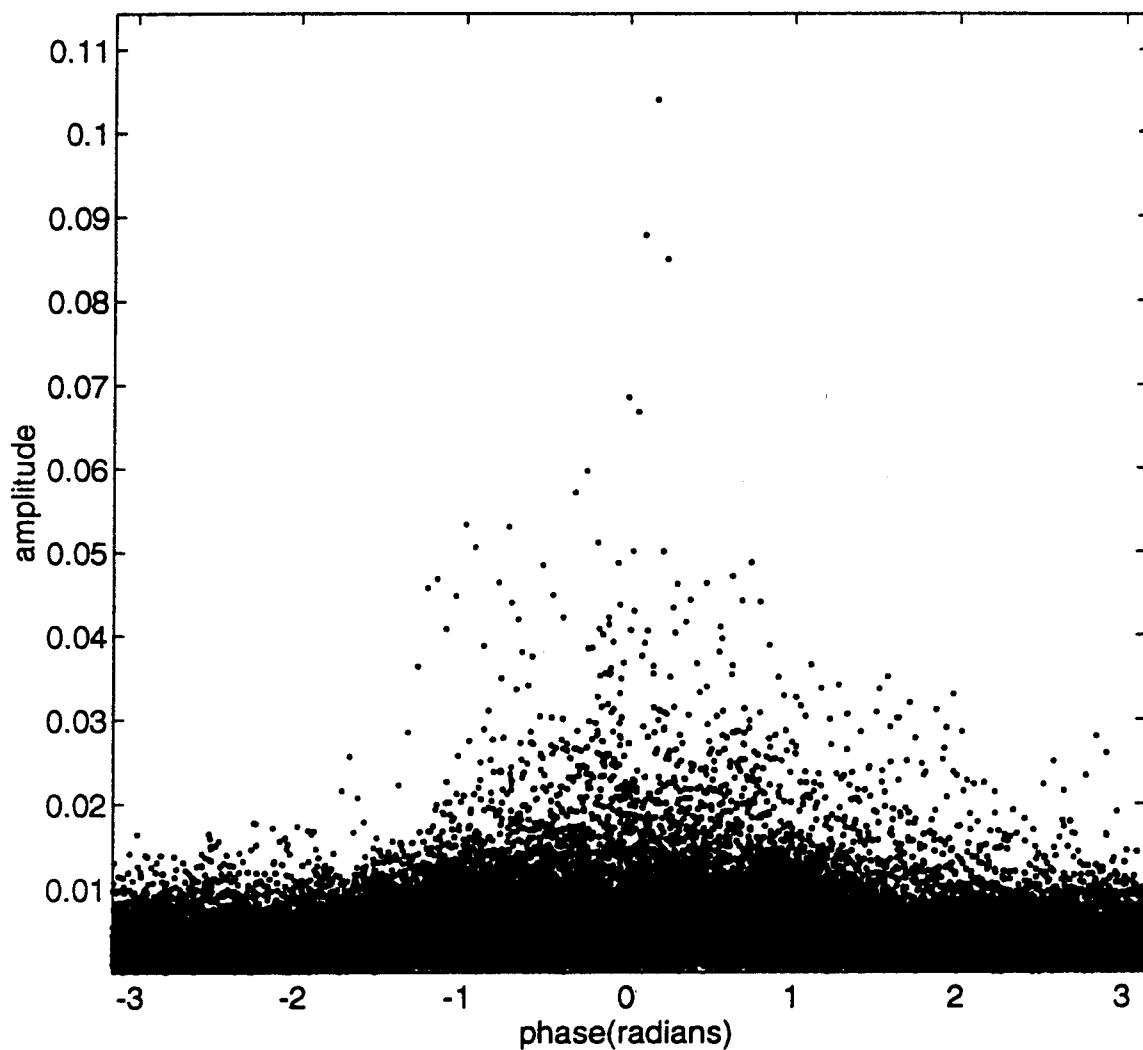


Figure 4-9. Amplitude of Chop vs Phase of Swell Scatter Diagram  
 Observe that the center of the mound of points above 0.015 amplitude is shifted slightly to the right possibly indicating that the maximum compressions of the chop lag slightly behind the crest of the swell



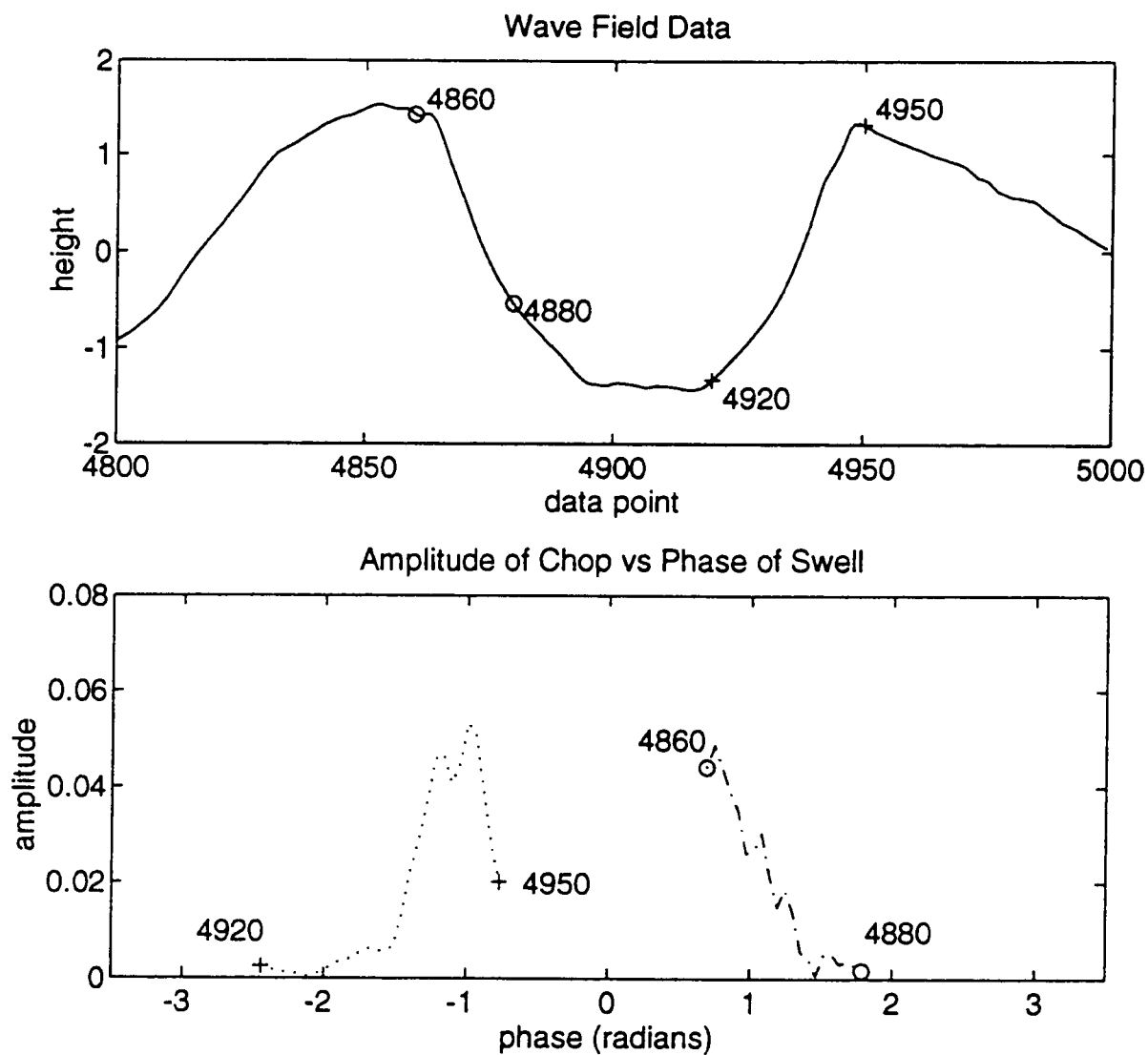


Figure 4-10. Original Wave and Sample Rare Events  
 In the top plot, the wave is moving from right to left. Event one from point 4860 to point 4880 is on the trailing side of a wave the crest of which has just passed the wave height staff. Event two from point 4920 to point 4950 is on the leading side of a wave the crest of which has not yet reached the wave height staff.

The events exhibit short bursts of high frequency of relatively high amplitude and are always near the crest of a wave. Their characteristics are similar to breaking waves. Additional information about the conditions at the time the data was taken will be required to resolve exactly what these events signify. More of the events found in this data set were of the first type where the crest of the wave had just passed the staff which would account for the central mass of the data points being slightly to the right of zero phase.

### **3. Distribution Plot - Wave Field Data**

When the first distribution plots were produced for the field data it was noticed that there were two distinct regions from about  $\pi/2$  to  $\pi$  and  $-\pi/2$  to  $-\pi$  where the density of points seemed to be much higher (see lower plot of Figure 4-11). Again we were optimistic that we had found evidence of the collective mode. However, this proved to be an artifact of the generally non-symmetric shape of water waves. Natural water waves tend to have sharply pointed crests so that when sampled at a constant rate there are more sample points in the troughs of the waves than near the crests. To compensate for this the distribution was normalized across the amplitude range by dividing the values in each column of the matrix by the sum of that same column. For each increment of phase the total density of points is the same.

Figure 4-11 shows the distribution of the amplitude of the chop versus the phase of the swell for the wave field data both before and after normalizing. The dominant feature of these plots is the large central mound. One possible explanation for this is that the chop amplitude is being compressed near the crests of the swell. In both of these plots, the shape of the distribution and of the rms amplitude curve are reminiscent of the zero phase shift plot for the test signal (see previous Figure 4-6).

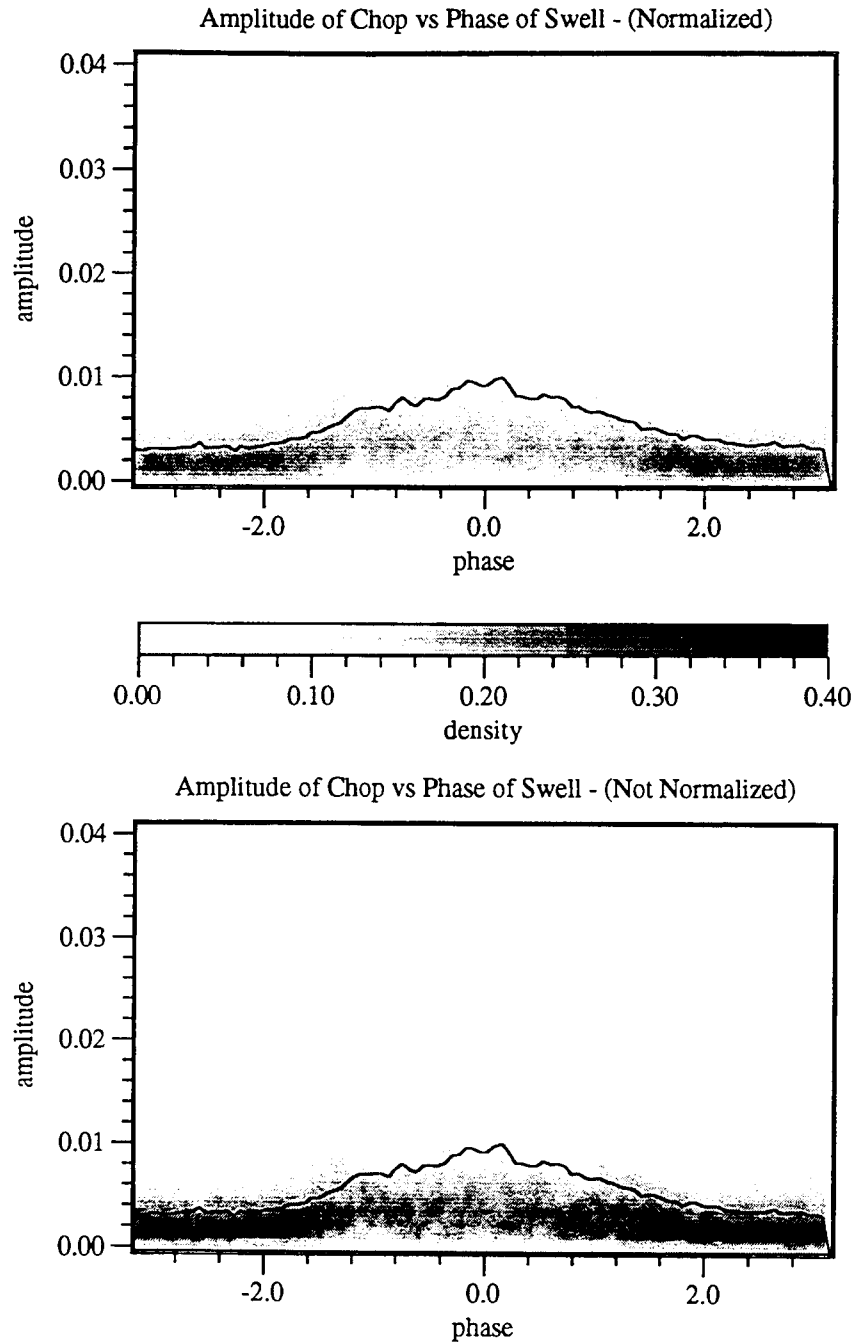


Figure 4-11. Distribution of Chop Amplitude vs Swell Phase - Wave Field Data  
The top plot shows the results of normalizing the amplitude distribution. This step was necessary to compensate for the generally non-symmetric shape of the water waves. Sampled at a constant rate relatively more points are taken in the troughs of the wave than are taken near the crests. This accounts for the denser areas in the lower plot where the distribution was not normalized.

#### **4. Frequency Octave Band Analysis - Wave Field Data**

For this part of the analysis, Chebyshev Type II band pass filters are used to filter the data into five octave bands. This was done in order to permit more precise identification of the frequencies and to allow comparisons to be made between adjacent and non-adjacent octave bands. The octave bands are band 1: 0 to 0.625 Hz, band 2: 0.625 to 1.25 Hz, band 3: 1.25 to 2.5 Hz, band 4: 2.5 to 5 Hz, and band 5: 5 to 10 Hz.

Figure 4-12 is a plot of the power spectrum of the wave field data and superimposed on the spectrum are the spectra of the five octave bands showing their relationship to each other.

In Figure 4-13 the amplitude of the chop (band 2) is plotted against the phase of the swell (band 1). This plot is very similar to the plot in Figure 4-11 which was observed to be similar to the plot of the test signal with zero phase shift from Figure 4-6.

Figure 4-14 shows the results of comparing the amplitude of chop bands 2,3,4, and 5 to the phase of swell band 1. Observe that the central mound becomes less pronounced as the octave separation increases but is still the most dominant feature of these plots indicating that the relationship noted in Figure 4-13 is not restricted to adjacent octave bands.

Figure 4-15 shows the results of comparing the amplitude versus phase of adjacent bands 3 and 2. Observe that there is no central mound and that the amplitude values appear to be uniformly distributed across all possible phase values.

Figure 4-16 shows the results of comparing the amplitude versus phase of the remaining octave bands 4 versus 2, 5 versus 2, 4 versus 3, and 5 versus 3. As noted in Figure 4-15, the central mound is not present and the amplitude values are uniformly distributed across the range of phase values.

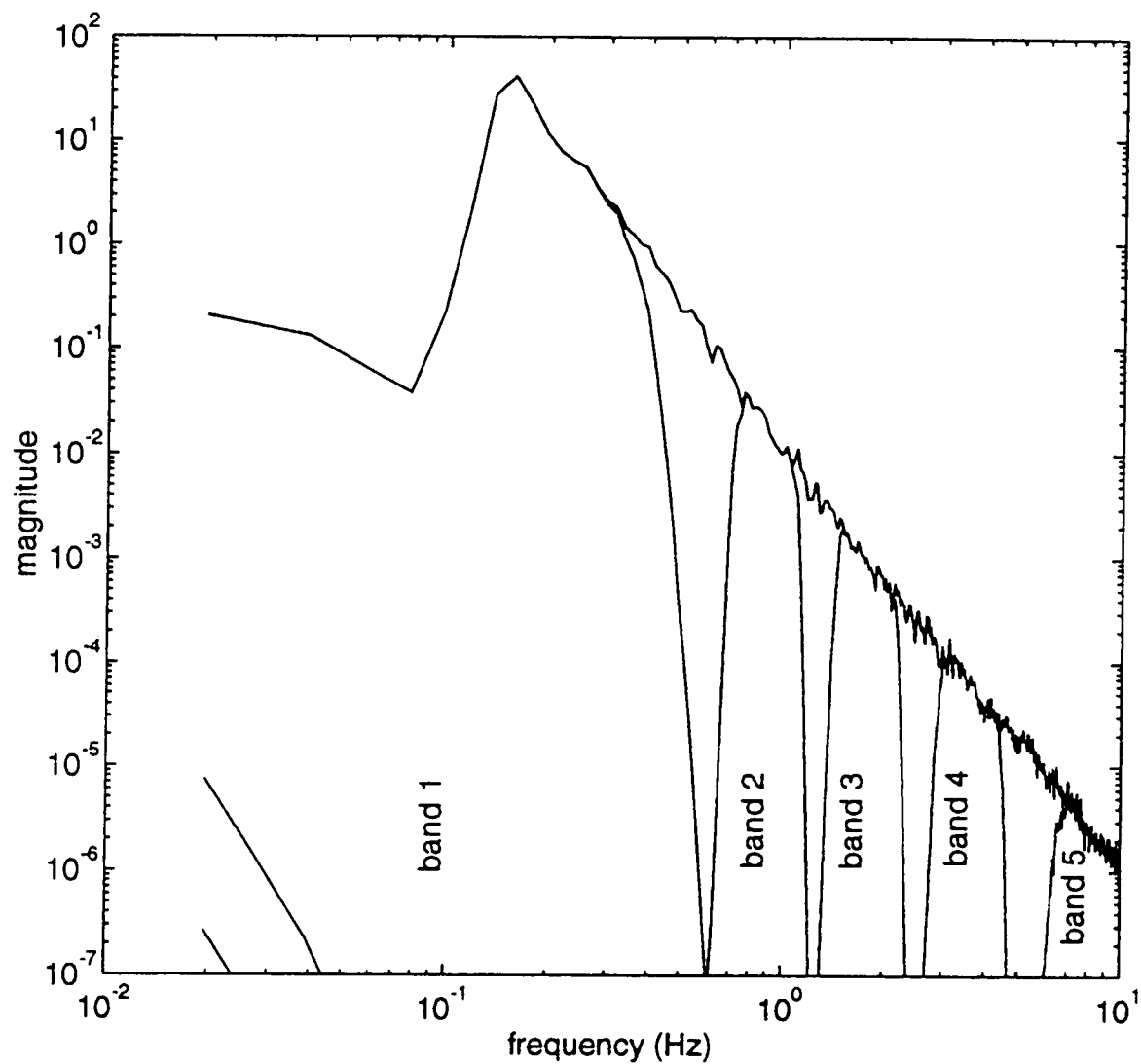


Figure 4-12. Power Spectra of Wave Field Data and 5 Octave Bands  
 Band 1 - 0 to 0.625 Hz.      Band 2 - 0.625 Hz to 1.25 Hz.  
 Band 3 - 1.25 Hz to 2.5 Hz.    Band 4 - 2.5 Hz to 5 Hz.  
 Band 5 - 5 Hz to 10 Hz.

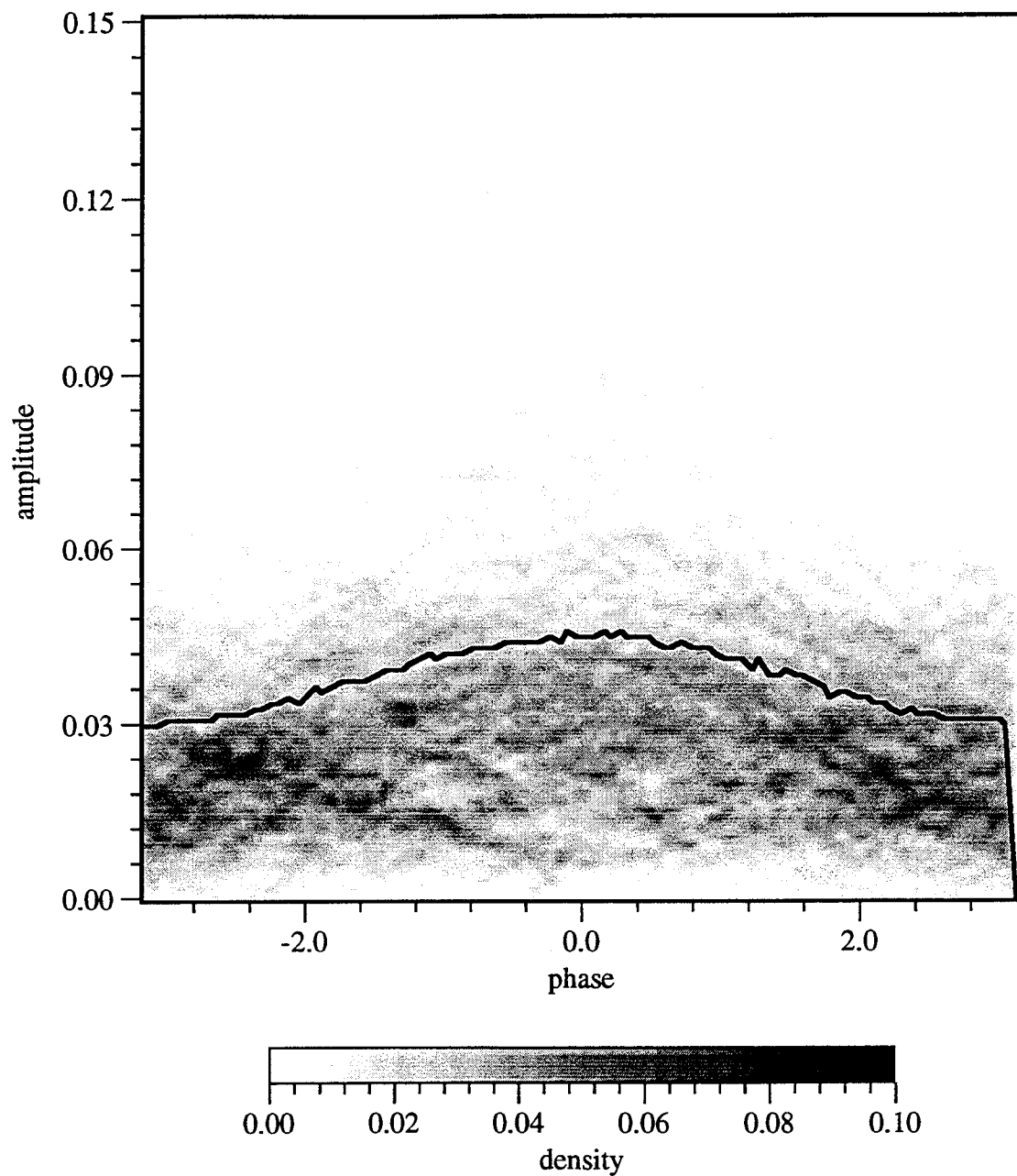


Figure 4-13. Amplitude of Chop vs Phase of Swell - Wave Field Data  
 This plot shows the distribution of the amplitude of the chop (band 2) versus the phase of the swell (band 1). The solid line is the RMS Amplitude of the Chop. Observe that there appears to be a relationship between the phase of the swell and the amplitude of the chop. Compare this plot with the phase shift 0 plot of the Test Signal on Figure 4-6.

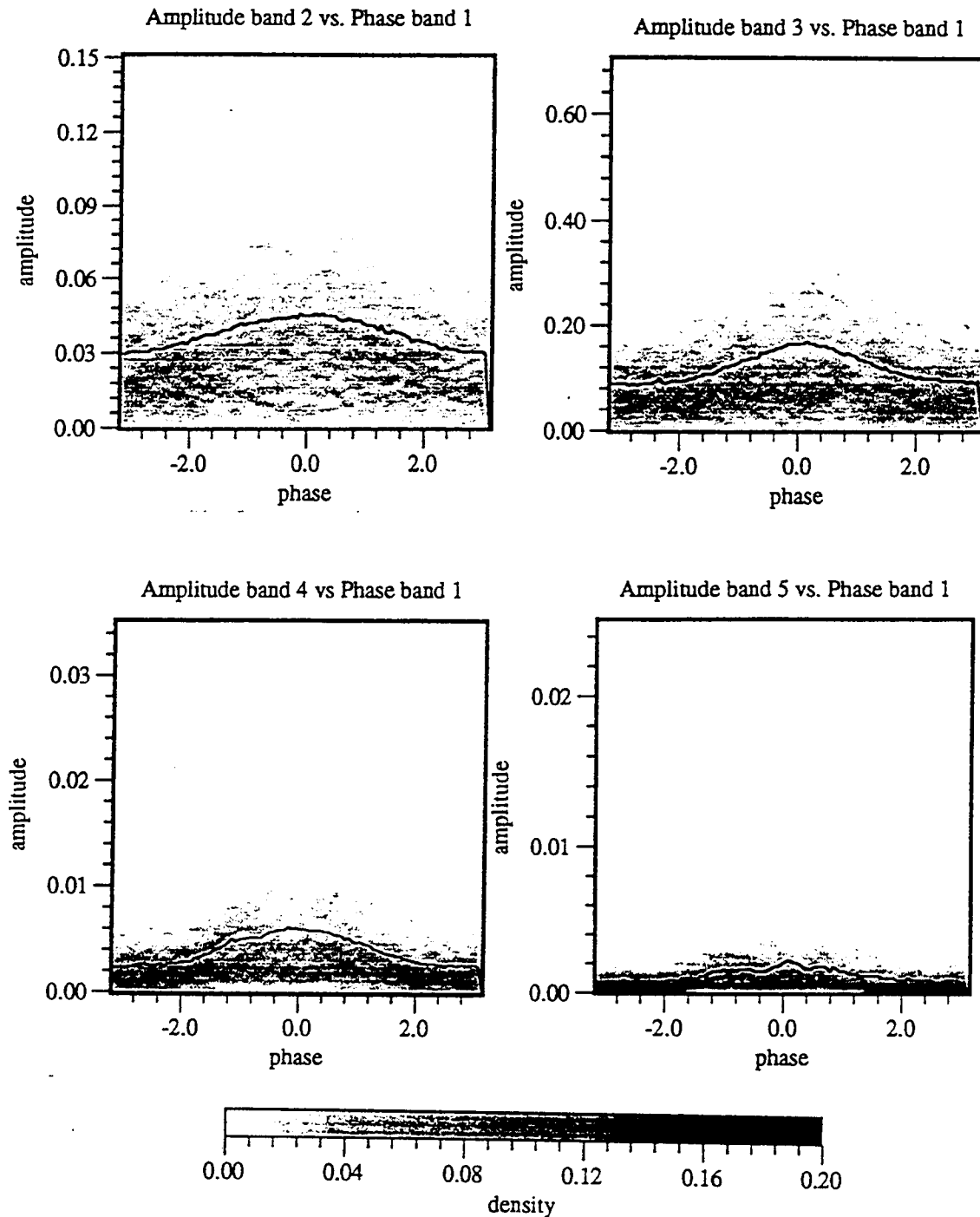


Figure 4-14. Amplitude of Chop Bands vs Phase of Swell - Wave Field Data  
 These plots compare the amplitude of the chop in bands 2 through 5 with the phase of the swell in band 1. Observe that the same relationship noted in Figure 4-13 (i.e. phase shift 0) is repeated as the band number increases indicating that this relationship is not limited to adjacent octave bands.

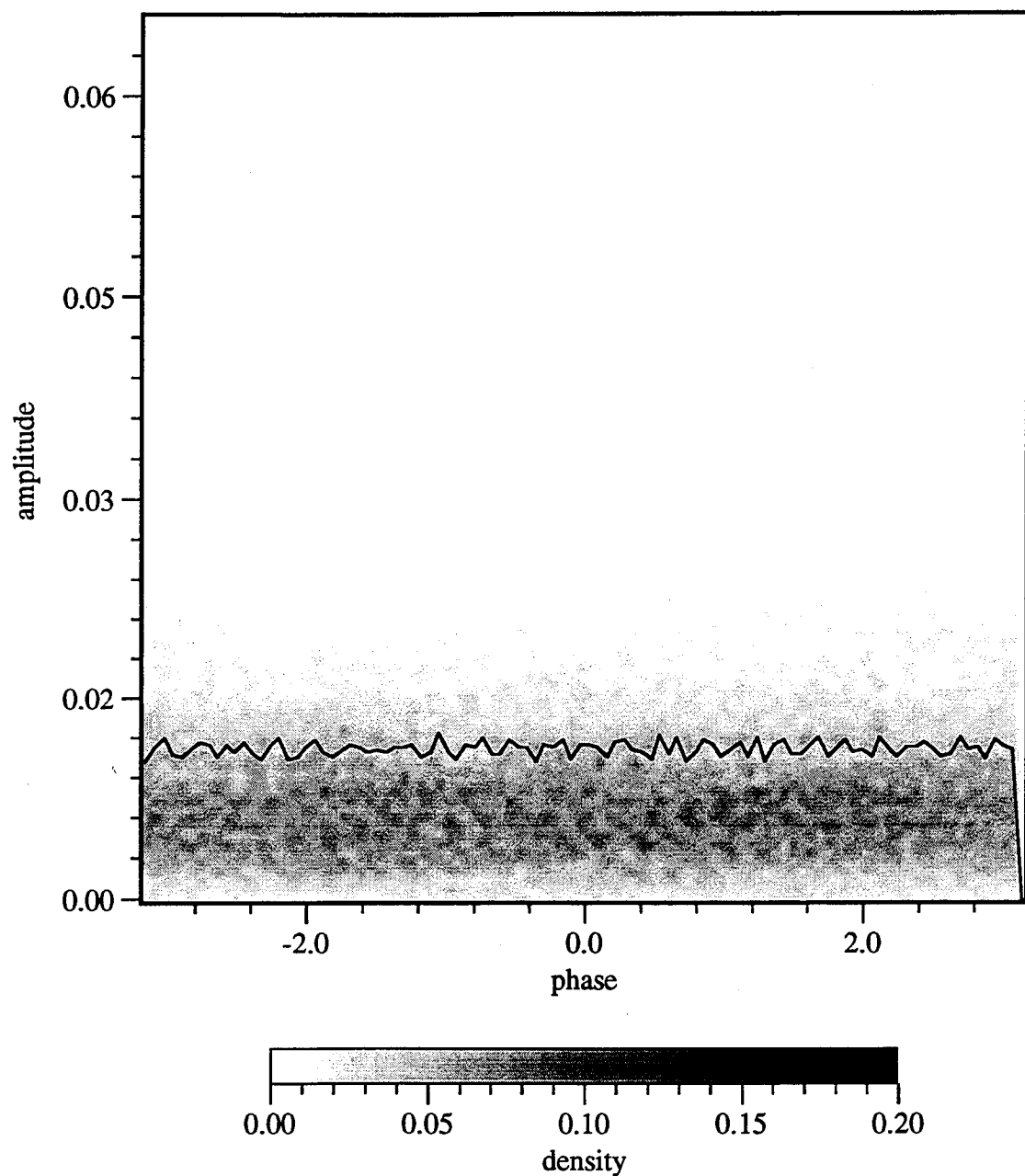


Figure 4-15. Amplitude of Chop vs Phase of Swell - Wave Field Data  
This plot shows the distribution of the amplitude of band 3 versus the phase of band 2. The solid line is the RMS Amplitude of band 3. Observe that the rms amplitude is essentially flat indicating a uniform random distribution of amplitude values across all possible phase values.



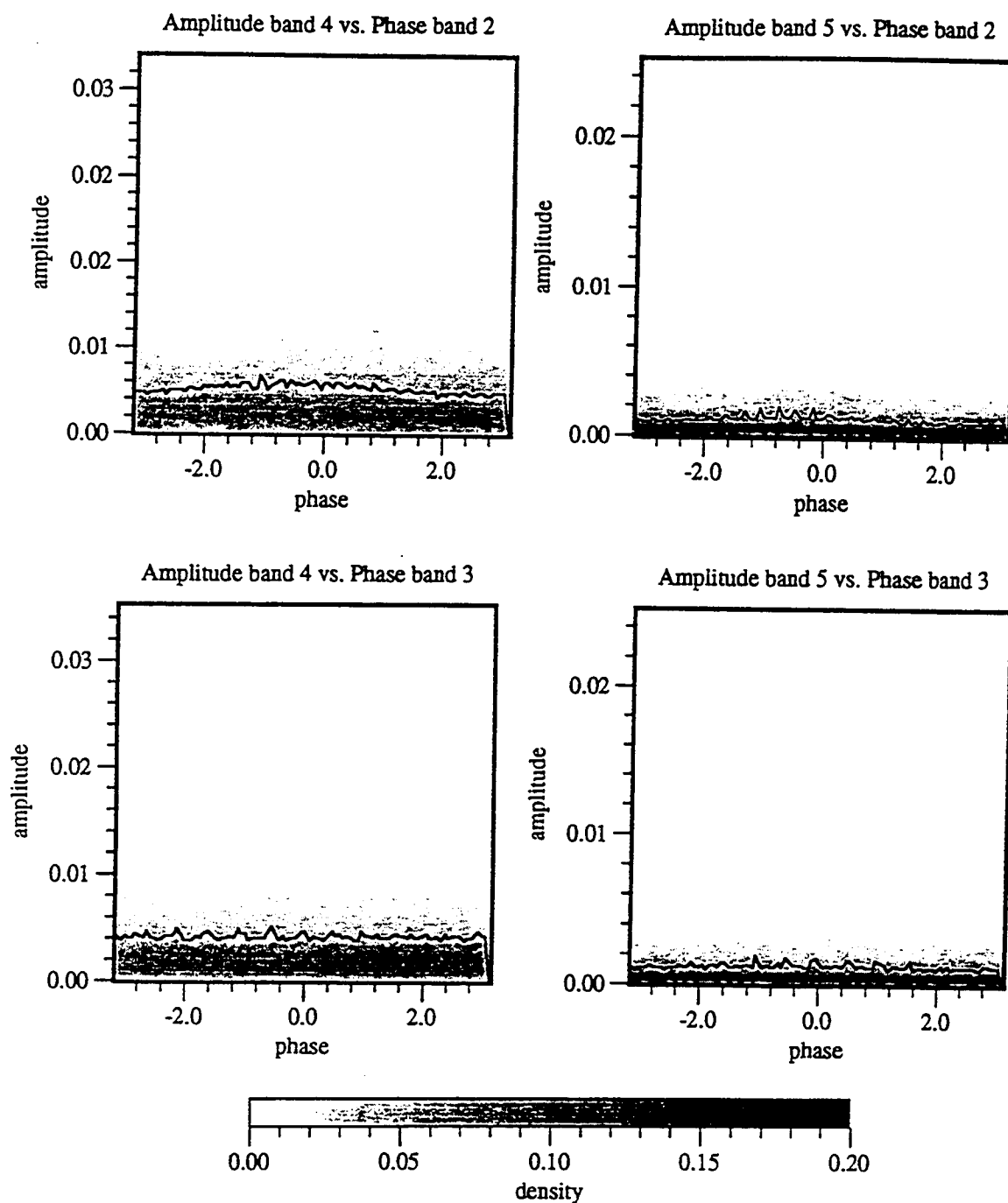


Figure 4-16. Amplitude vs Phase - Wave Field Data

These plots show the amplitude of bands 4 and 5 plotted against the phase of bands 2 and 3. Observe that as noted in Figure 4-15, the amplitude values show a uniform random distribution across all possible phase values.

## 5. Filtering - Wave Tank Data

The wave tank data was filtered into swell and chop components using the same procedure as described for the field data. However, the tank data differs from the previous field data in that the "swell" is imposed at a specific frequency, 0.068 Hz corresponding to the fundamental mode of the tank. The low pass cutoff frequency was adjusted to 0.2 Hz to capture the swell frequency.

Figure 4-17 shows the first 1000 points of the original wave tank data, the low wave or swell component output from the low pass filter and the high wave or chop component output from the high pass filter. Figure 4-18 shows the power spectra of these three waves and illustrates how they relate to each other in the frequency domain.

## 6. Distribution Plot - Wave Tank Data

The first attempt to produce a distribution plot of the tank data resulted in Figure 4-19. There were essentially no points with phase values beyond  $\pm\pi/2$ . The problem was that the Hilbert transform was seeing a small phase variation riding on top of a large dc value. In order to establish a reference for determination of the true phase of the swell, the dc component (mean) was subtracted from the data set as the first step in analysis. The result is shown in Figure 4-20. The extra step of subtracting the mean from the wave data was incorporated into the processing of the field data as well. All of the previous results for the field data have included this step.

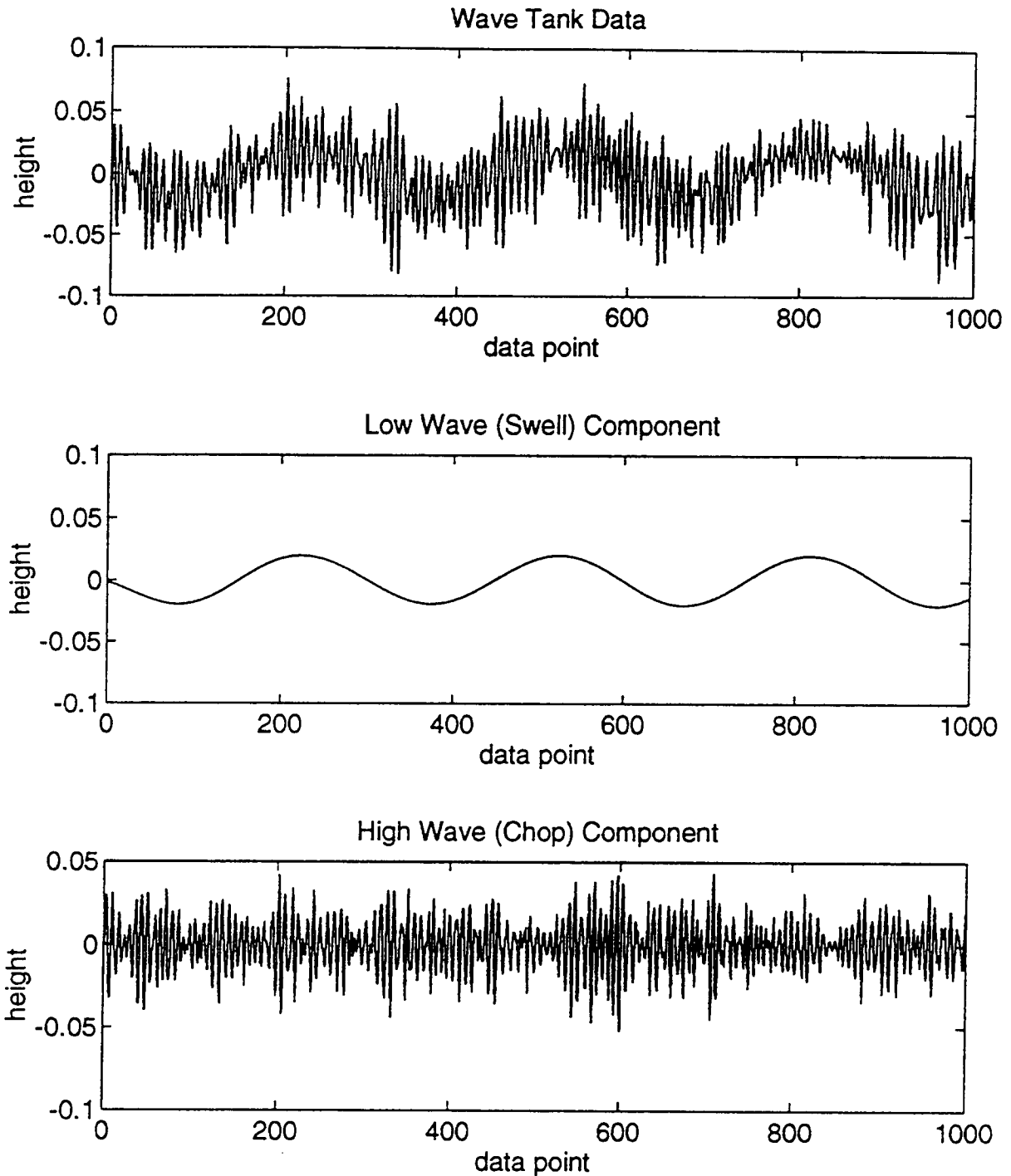


Figure 4-17. Wave Tank Data, Low Wave (Swell), and High Wave (Chop). Swell is output of Low Pass Chebyshev Type II filter. Chop is output of High Pass Chebyshev Type II filter. Only the first 1000 points of each sequence are plotted.

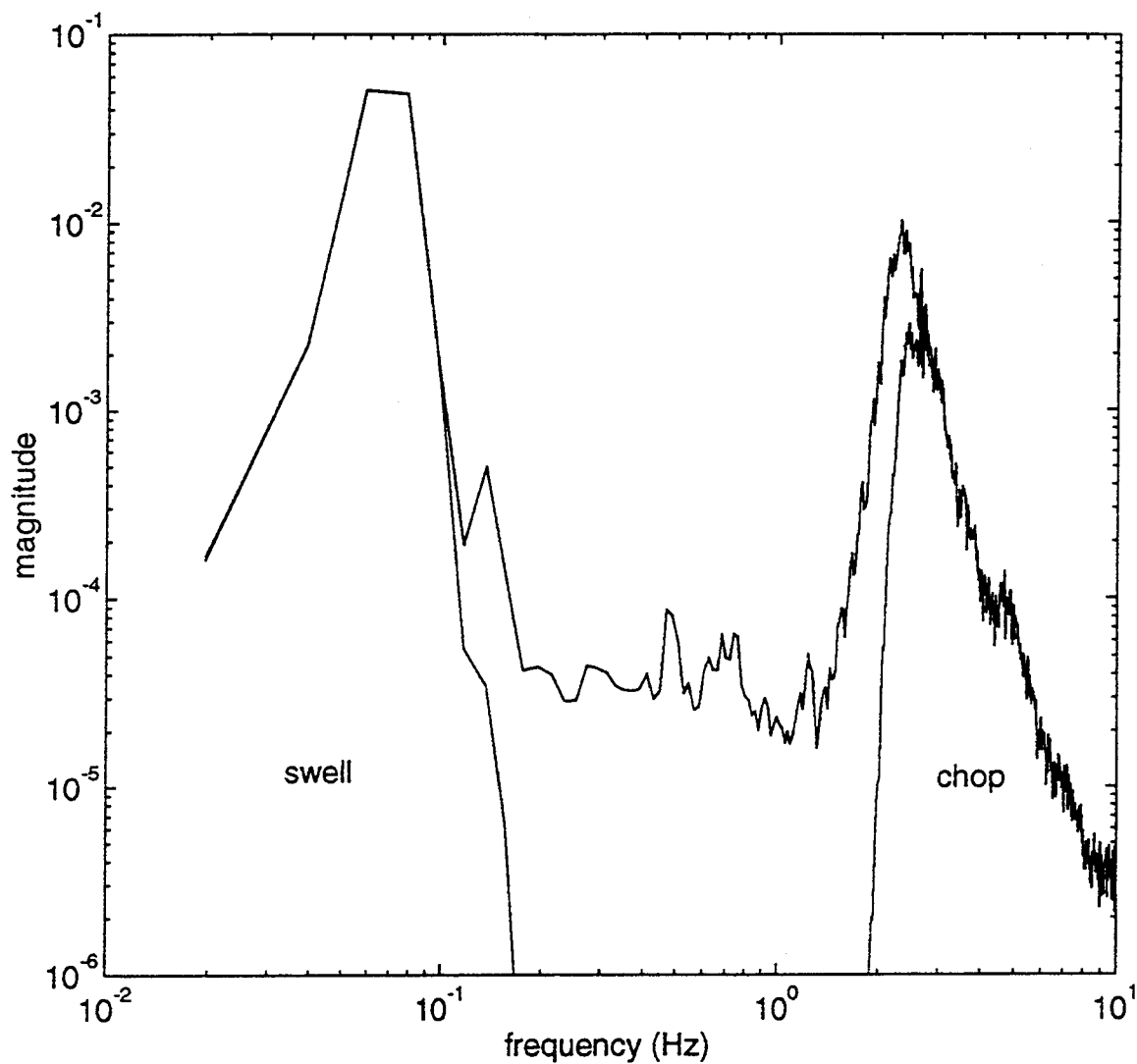


Figure 4-18. Power Spectra of Wave Tank Data, Swell and Chop  
Location of the swell and chop components of the tank data are indicated by their respective power spectra. Cutoff frequency for the swell is 0.2 Hz. Cutoff frequency for the chop is 1.5 Hz.

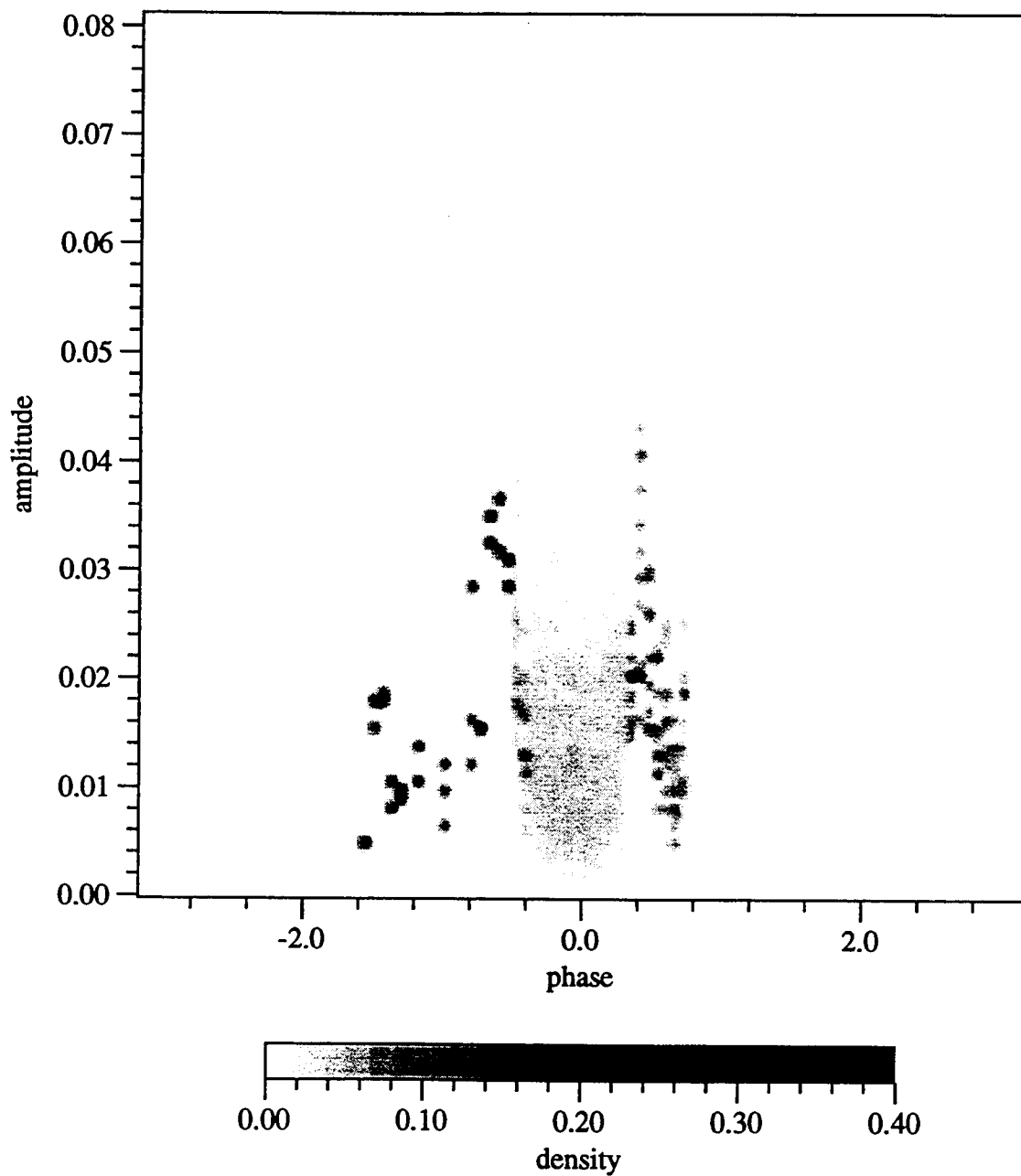


Figure 4-19. Distribution Plot of Amplitude vs Phase - Wave Tank Data.  
 In this plot the dc or mean of the data has not been subtracted from the sequence.  
 Compare this plot with Figure 4-20 where the dc has been subtracted.

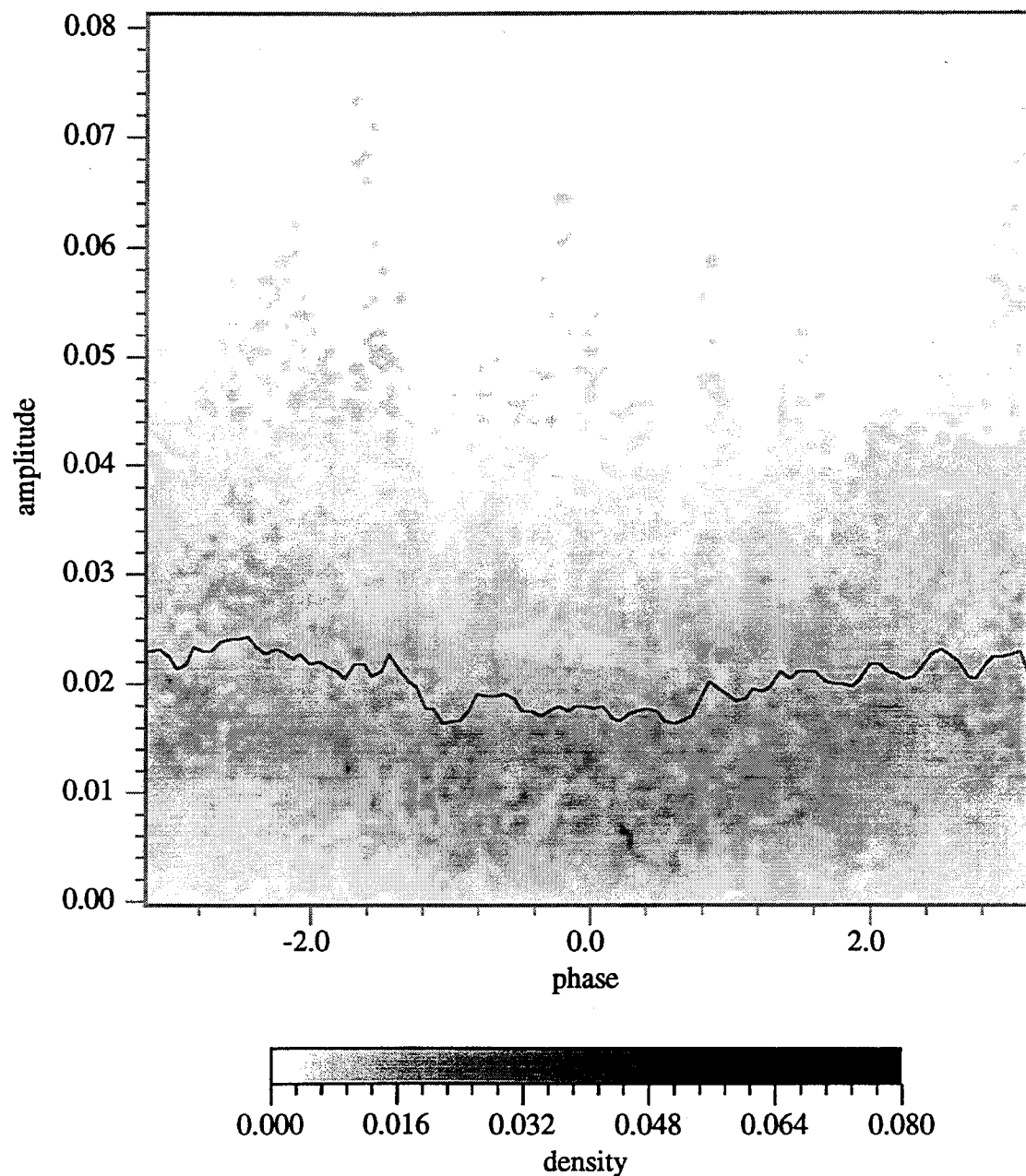


Figure 4-20. Distribution Plot of Amplitude vs Phase - Wave Tank Data. In this plot the dc or mean of the data has been subtracted from the sequence. The solid line is the RMS amplitude of the chop. Observe that this plot has two maxima much like the plot of the Test Signal with a 180 degree phase shift between the phase of the swell and the amplitude of the chop (see Figure 4-6).

Figure 4-20 shows the distribution of the amplitude of the chop versus the phase of the swell for the wave tank data. This provides the strongest evidence in this investigation in support of the collective mode. Here the collective mode, represented by the modulation of the chop, is being driven above its natural frequency of oscillation by the swell. As a result the modulations are lagging the swell by 180 degrees.

Some concern was expressed that the above result might have been caused by an inversion of the measurements taken in the tank. In Appendix B, an experiment is described which demonstrated that this was not the case.

## V. CONCLUSIONS AND FUTURE WORK

The FFT approach did not concurrently provide adequate resolution in the time and frequency domains to permit direct comparison of the phase of the lower swell frequencies with the compressions of the higher chop frequencies. This approach is therefore not recommended for further use in investigating wave turbulence.

The Hilbert Transform approach in combination with the digital signal filtering appears to provide the necessary flexibility to handle a variety of data. The results obtained with the field data and tank data are consistent with the test signal results thus providing confidence that the method is presenting a true picture of the physics.

The analysis of the wave field data as yet provides no clear evidence to support or refute wave turbulence theory. The analysis of the wave tank data, on the other hand, appears to indicate a 180 degree phase shift between the modulation of the chop amplitude and the phase of the swell, which supports the presence of a collective mode.

However, both of these observations are based on only one data set each. Additional data sets taken under various conditions will need to be analyzed and the Hilbert Transform method described above seems to hold the best promise.





## APPENDIX A. MATLAB CODE

This appendix contains the Matlab code used to perform the Hilbert Transform analysis of the wave field data and with minor modification the analysis of the wave tank data as well.

```
% file is run_lake_cheby2.m
% runs in sequence the programs to analyze wave data
clc;
wave1 = input('Enter name of wave vector to process >> ');
samp_freq = input('Enter sample frequency >> ');
nyq_freq = samp_freq/2; % nyquist frequency
power_spec      % estimate power spectrum of wave
% remove dc component from wave data
wave1 = wave1 - mean(wave1);
% Note: cutoff frequencies for filters are hard coded
% change them below if different values are desired.
cf_low = 0.625;  % cutoff frequency low
cf_high = 1.5;   % cutoff frequency high
cheby2_low      % filter low wave
cheby2_high      % filter high wave
hilbert_phase_low % hilbert transform to get phase of low wave
hilbert_ampl_high % hilbert transform to get amplitude of high wave
amp_vs_phase_den % calculate density of amplitude of high vs phase of low
% save matrices for later plotting with Spyglass Transform program
save lake2 M -ascii
save rmslake2 rms_amp -ascii
```

```

% file is power_spec.m
% normally run as sub-program from a runner program
% like run_lake_cheby2.m.
% This file calculates and plots the power spectrum of the wave
% data. A default Hanning window is used. The window length is
% set to 1024. A loglog plot is produced.
% Warning : load wave data before running this script
[Pwave,fwave] = psd(wave1,1024,samp_freq); % default window is hanning
figure('PaperPosition',[0.90 3.05 6.95 6.1]); clf;
loglog(fwave,Pwave); hold on;
%title('Power Spectrum Estimate of Wave Data');
xlabel('frequency (Hz)');
ylabel('magnitude')
% save axes settings for later spectrum plots of filtered data
laxes = axis;
%add omega^-4 line for comparison
p=(2*pi*fwave).^(-4);
loglog(fwave,p); axis(laxes);
pause(5);

% file is cheby2_low.m
% build low pass chebyshev type 2 filter
% type - chebyshev type 2 order - 5
% stop band attenuation - -40dB cutoff frequency - cf_low
[b,a]=cheby2(5,40,cf_low/nyq_freq); % default is low pass filter
% examine frequency response
[h,w]=freqz(b,a,512);
figure; clf;
loglog(10*(w/pi),abs(h).^2)
title('Magnitude-Frequency Response of Low Pass Chebyshev Type 2 Filter')
xlabel('frequency (Hz)'); ylabel('normaliized magnitude (dB)');
pause(5);
% filter data using non-causal zero phase filtering
low_wave=filtfilt(b,a,wave1);

```

```

maxlow=max(low_wave);
% examine spectrum of the low wave using same settings
% as for spectrum of original -- to allow comparison
% uses same axis settings saved from power_spec.m
[P,f] = psd(low_wave,1024,samp_freq);
figure; clf;
loglog(f,P); axis(laxes);
title('Power Spectrum Estimate of Low Wave');
xlabel([' frequency (Hz) - cutoff frequency ',num2str(cf_low),' Hz']);
ylabel('magnitude (dB)');
pause(5);

% file is cheby2_high.m
% build high pass chebyshev type 2 filter
% type - chebyshev type 2 order - 5
% stop band attenuation - -40dB cutoff frequency - cf_high
[b,a]=cheby2(5,40,cf_high/nyq_freq,'high');
% examine frequency response
[h,w]=freqz(b,a,512);
figure; clf;
loglog(10*(w/pi),abs(h).^2);
title('Magnitude-Frequency Response of High Pass Chebyshev Type 2 Filter')
xlabel('frequency (Hz)'); ylabel('normalized magnitude (dB)');
pause(2);
% filter data using non-causal zero phase filtering
high_wave=filtfilt(b,a,wave1);
maxhigh=max(high_wave);
% examine spectrum of the high wave using same settings
% as for spectrum of original -- to allow comparison
% uses same axis settings saved from power_spec.m
[P,f] =psd(high_wave,1024,samp_freq);
figure; clf;
loglog(f,P); axis(laxes);

```

```

title('Power Spectrum Estimate of High Wave');
xlabel(['frequency (Hz) - cutoff frequency ',num2str(cf_high),' Hz']);
ylabel('magnitude (dB)');
pause(5);

```

```

% file is hilbert_phase_low.m
% takes hilbert transform of low_wave and calculates
% instantaneous phase angle between -pi and +pi
hilbert_low = hilbert(low_wave);
phase_low= angle(hilbert_low);

```

```

% file is hilbert_ampl_high.m
% takes hilbert transform of high_wave and calculates
% instantaneous amplitude which provides us with a measure
% of the compression of the high frequencies
hilbert_high= hilbert(high_wave);
amp_high = abs(hilbert_high);

```

```

% file is amp_vs_phase_den.m
% Calculates the density of amplitude of high vs phase of low
% falling in cells of a L by L matrix. The columns are normalized.
% Normalized data is used as input to Transform program for
% final production of density plots.
% The rms amplitude is calculated for later plotting in Transform.
L = 100;
N = length(phase_low);
phase_scale= linspace(-pi, pi, L);
amp_scale = linspace(0, 1.1*max(amp_high),L);
M = zeros(L,L);
for n = 1:N
    col = min(find(phase_low(n)<phase_scale))-1;

```

```

row = min(find(amp_high(n)<amp_scale))-1;
M(row,col) = M(row,col) + 1;
end;
M(1,100) = 1; % dummy value to avoid division by zero
ampsqu = amp_scale.^2;
% normalize amplitude weights across phase values
% and calculate rms amplitudes by phase
for n=1:100
NormM(n,:) = M(n,:) ./ sum(M);
rms_amp(n)=sqrt(sum(M(:,n).*ampsqu')/sum(M(:,n)));
end;
NormM(1,100) = 0; % reset dummy value
rms_amp(100)=0;

```



## APPENDIX B. WAVE TANK SIGN TEST

In a continuing effort to track down and eliminate, if possible, potential sources of error, an experiment was conducted to ensure that the circuitry of the wave height measurement system employed at the Ocean Wave Acoustic Facility at NPS and my software had not introduced an inversion error. If such an error had been introduced the picture presented in Figure 4-20 would have been reversed with the maximum chop amplitude occurring at the crest of the swell.

The experiment consisted of manually pushing the wave height probe down into the tank of still water to simulate being at the crest of the wave and then jiggling it up and down to simulate the chop riding on top of the swell . At a time chosen to simulate a long slow swell the probe was withdrawn thus simulating the trough of the swell. The probe was held as still as possible for this period to simulate little or no chop in the trough.

Figure B-1 shows the time domain plot of the result of processing this data using the programs in this thesis. By comparing the two lower plots one can see that the largest amplitude modulations of the simulated chop are occurring at the crests of the simulated swell. Figure B-2 shows the distribution plot of the amplitude of the chop and the phase of the swell along with the rms of the amplitude. The plot clearly show the largest chop amplitude is occurring at the crests of the swell thus verifying that the measurements taken in the wave tank do not contain an inversion error.



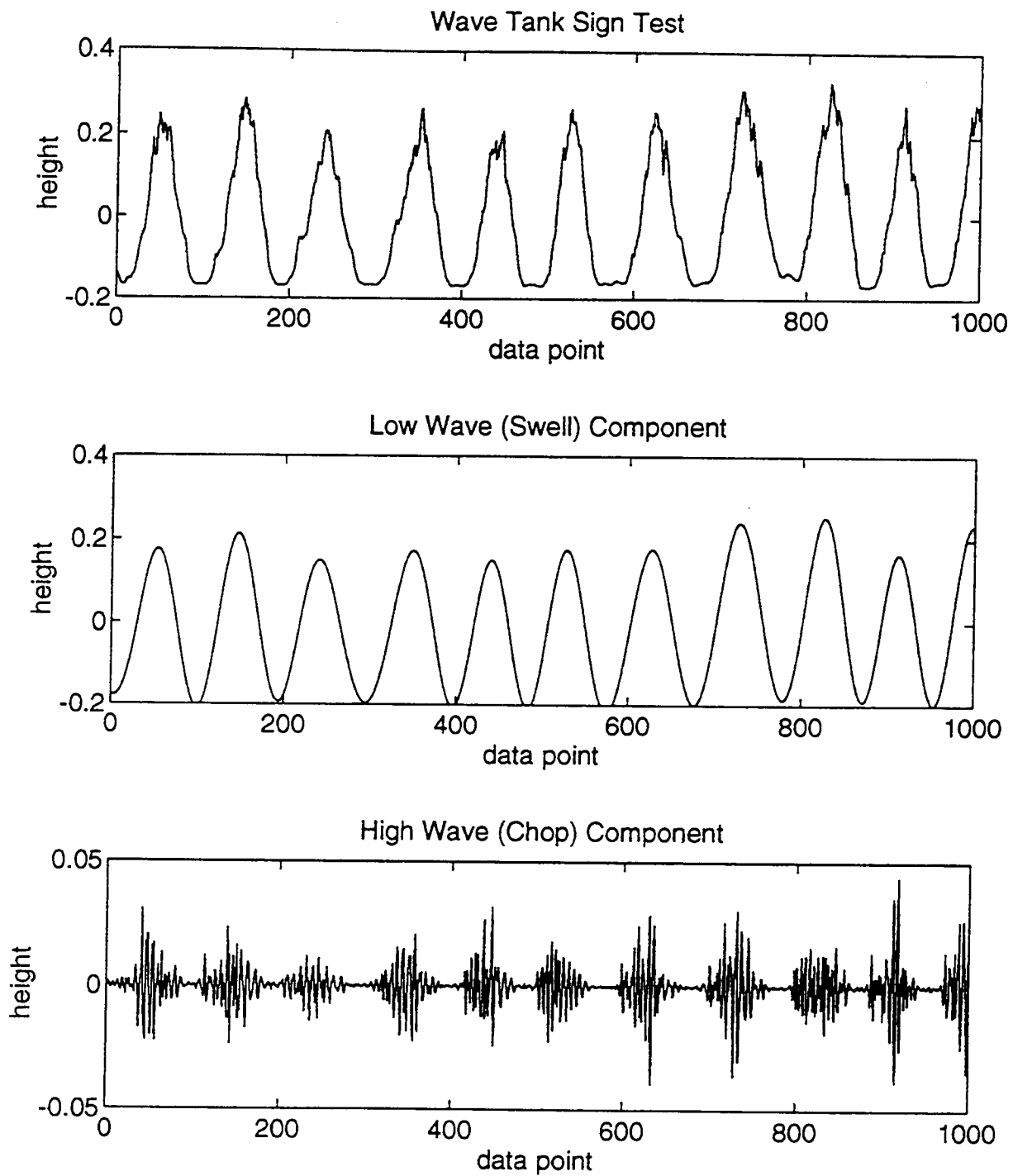


Figure B-1. Wave Tank Data Sign Test.  
Swell cutoff frequency is 0.5 Hz. Chop cutoff frequency is 1.5 Hz.  
Only the first 1000 points of each sequence are plotted.

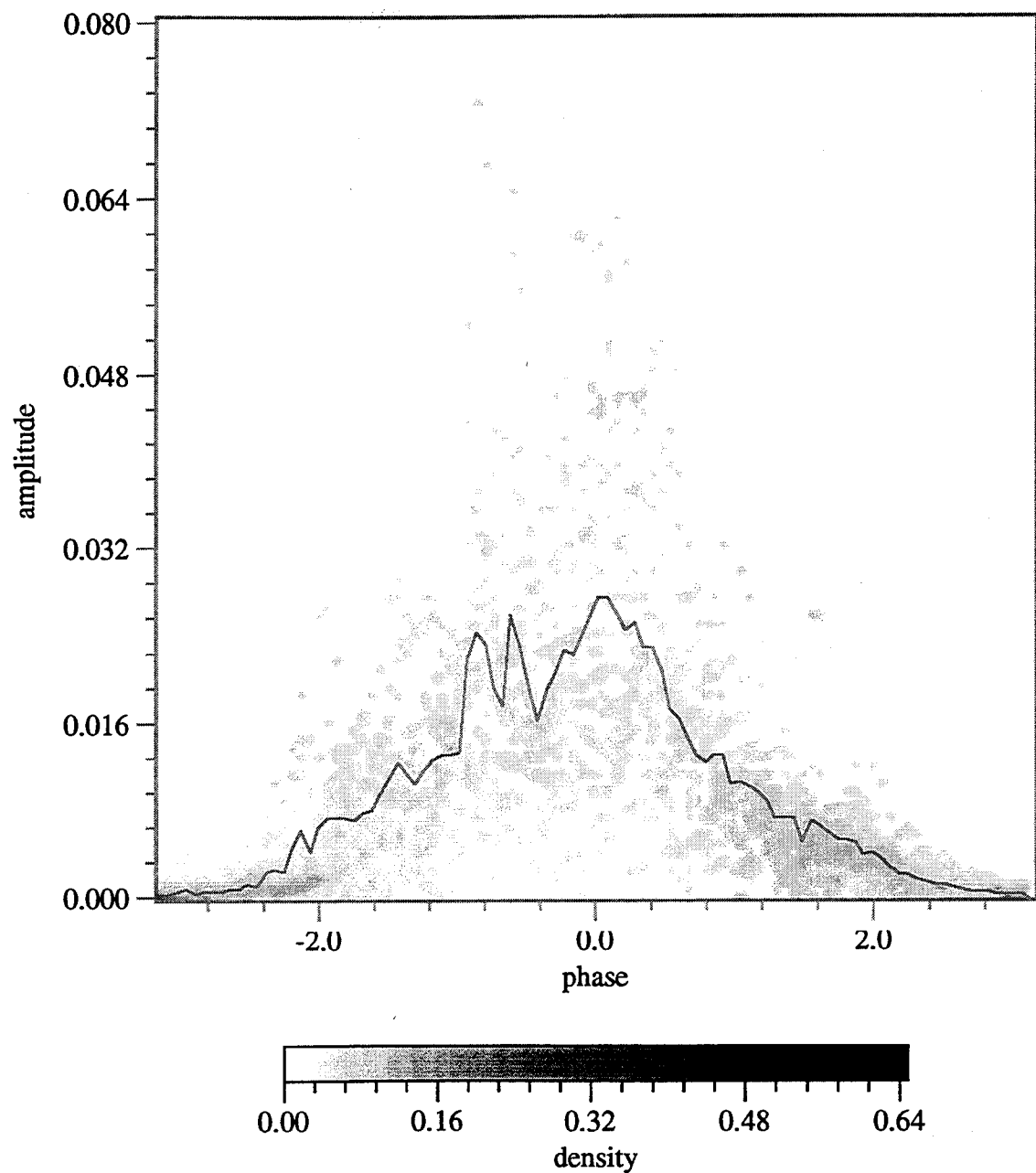


Figure B-2. Distribution Plot of Amplitude vs Phase - Wave Tank SignTest. The solid line is the RMS amplitude of the chop. The largest chop amplitude is occurring at the crests of the swell thus verifying that the measurements taken in the wave tank do not contain an inversion error.



## REFERENCES

- (Donelan, 1985) Donelan, M.A., Hamilton, J., and Hui, W.H., "Directional Spectra of Wind-Generated Waves," *Phil. Trans. R. Soc. Lond. A*, 315, pp. 509-562, 1985.
- (Forristall, 1981) Forristall, G.Z., "Measurements of a Saturated Range on Ocean Wave Spectra," *J. Geophys. Res.* Vol. 86, pp. 8075-8084, 1981.
- (Haykin, 1983) Haykin, S., *Communication Systems*, Second Edition, John Wiley and Sons, Inc., New York, 1983.
- (Larrazza, 1990) Larrazza, A., Garrett, S.L. and Putterman, S., "Dispersion Relations for Gravity Waves in a Deep Fluid: Second Sound in a Stormy Sea," *Phys. Rev. A* 41, pp. 3144-3155, 1990.
- (Larrazza, 1993) Larrazza, A. and Falkovich, G., "Collective Modes in Open Systems of Nonlinear Random Waves," *Phys. Rev. B* Vol. 48, No. 13, pp 9855-9857, 1993.
- (Lawrence, 1992) Lawrence, R. "Experimental Inquiries Into Collective Sea State Modes in Deep Water Gravity Waves," Masters Thesis, Naval Postgraduate School, Monterey, CA, December 1992.
- (Mathworks, 1992) *Matlab Reference Guide*, The Mathworks Inc., Natick, MA, 1992.
- (Mathworks, 1993) *Signal Processing Toolbox User's Guide*, The Mathworks Inc., Natick, MA, 1993.
- (Spyglass, 1993) *Spyglass Transform Quick Tour and Reference*, Version 3.01, Fourth Edition, Spyglass, Inc., Champaign, IL, 1993.
- (Zakharov, 1992) Zakharov, V., Lvov, V., Falkovich, G., "Kolmogorov Spectra of Turbulence," *V.1 Wave Turbulence*, Springer-Verlag, 1992.



## INITIAL DISTRIBUTION LIST

		No. Copies
1.	Defense Technical Information Center Cameron Station Alexandria, Virginia 22304-6145	2
2.	Library, Code 52 Naval Postgraduate School Monterey, California 93943-5002	2
3.	Professor Robert M. Keolian Physics Department, (Code PH/Kn) Naval Postgraduate School Monterey, California 93943	2
4.	Professor Andres Larraza Physics Department, (Code PH/La) Naval Postgraduate School Monterey, California 93943	1
5.	Dr. Michael F. Shlesinger Office of Naval Research, (Code 331) 800 N. Quincy Street Arlington, Virginia 22217-5660	1
6.	LCdr John P. Davies 1215 Tara Drive Ottawa, Ontario, Canada K2C 2H4	1
7.	Director of Naval Requirements National Defence Headquarters Ottawa, Ontario, Canada K1A 0K2	1
8.	Dr. Mark A. Donelan National Water Research Institute, Canada Centre for Inland Waters, Burlington, Ontario, Canada L74 4A6	1
9.	Professor Gregory Falkovich Department of Physics Weizmann Institute of Science Rehovot 76100, Isreal	1